Intended and Unintended Consequences of Atmospheric Methane Oxidation Enhancement

Hannah M. Horowitz[1]
[1] Department of Civil and Environmental Engineering and Department of Climate, Meteorology, & Atmospheric Sciences, University of Illinois Urbana-Champaign, Urbana, Illinois, USA

Correspondence to: Hannah M. Horowitz (hmhorow@illinois.edu)

Abstract. Atmospheric oxidation enhancement (AOE) of methane via either tropospheric hydroxyl radicals (OH) or chlorine (Cl) radicals is being considered as a method to decrease greenhouse gas concentrations. The chemistry involved is coupled; is nonlinear; and affects air quality, other greenhouse gases, and ozone-depleting substances. Here I perform a suite of experiments in a three-dimensional (3D) atmospheric chemistry model representing different OH- and Cl-based atmospheric oxidation enhancement methods, to estimate the effectiveness of each at decreasing greenhouse gases and the impacts on air quality and stratospheric ozone. I find that larger emissions of iron salt aerosol are required relative to previous work ~~may not be effective at~~to reduc~~ing~~ methane on a global scale by at least a few percent (≥565 Tg/yr), which indicates uncertainty in predicting the effectiveness of this method depending on the representation of the reaction mechanism and modeling framework employed. More work is needed to understand the kinetics of chlorine release from iron salt aerosol and the potential for bromine co-release, which ~~further~~ decreases effectiveness. Hydrogen peroxide–based approaches can decrease global methane, but the hydrogen peroxide emissions required may be too large to be feasible. I find that limiting emissions to daytime for hydrogen peroxide–based scenarios has negligible effects. All methods increase surface particulate matter (PM) pollution and in some regions lead to exceedances of annual air quality standards. Cl-based methods decrease ozone air pollution, but OH-based methods increase ozone air pollution in populated areas. While Cl-based methods can increase ozone-depleting substances, the 1-year timeframe of this study is insufficient to ~~I~~ predict ~~minimal changes in~~ impacts on stratospheric ozone ~~after 1 year of deployment~~. The overall impacts of atmospheric oxidation enhancement methods on climate and human health involve not only their effectiveness at decreasing methane, but competing or complementary effects on other greenhouse gases and aerosol, as well as varying effects on surface air pollution~~multiple competing factors~~.

1 Introduction

To achieve aggressive reductions in the greenhouse gas methane needed to reach climate goals, alternate strategies to emissions mitigation are being considered (NASEM, 2024). These include processes to decrease the atmospheric lifetime of methane by enhancing its main sinks (e.g., Abernethy et al., 2023; Gorham et al., 2024~~3~~; Li, Meidan, et al., 2023; Ming et al., 2022; Wang et al., 2022), using oxidation by tropospheric OH (currently >90%) and tropospheric Cl (currently 1–5%) (Allan et al., 2007; Gromov et al., 2018; Hossaini et al., 2016; Platt et al., 2004; Wang et al., 2019, 2021). ~~(e.g., Abernethy et al., 2023; Gorham et al., 2023; Li, Meidan, et al., 2023; Ming et al., 2022; Wang et al., 2022)~~. There are interactions between

Cl and OH; namely, increasing Cl decreases OH due to reductions in ozone (e.g., Horowitz et al., 2020; Li, Meidan, et al., 2023). In addition, Cl and OH can impact aerosol particles, other greenhouse gases, and ozone-depleting substances. Due to these interactions and the highly nonlinear chemistry involved, detailed atmospheric chemical investigations are needed to understand the overall climate and pollution impacts of methods to enhance atmospheric methane oxidation. To have the greatest impact on atmospheric methane, methods appropriate for ambient concentrations (≤ 2 parts per million) are needed, but the technology is not yet available (Abernethy et al., 2023; NASEM, 2024; Pennacchio et al., 2024).

While commercial OH generators exist on a smaller scale (e.g., to remove volatile organic carbon pollution; Johnson et al., 2014), it is less well understood how to scale up the artificial production of OH globally (e.g., Ming et al., 2022). Potential technologies could involve the release of hydrogen peroxide, downdraft energy towers, and/or artificial ultraviolet (UV) radiation (Tao et al., 2023; Wang et al., 2022). One specific method to release Cl atom is iron salt aerosol (e.g., Oeste et al., 2017), where the presence of both iron (III) and chloride enhances photolytic Cl atom release. Photolytic Cl atom release from artificial salts has been demonstrated in chamber experiments using salt pans and artificial sea salt aerosols generated from sodium chloride (NaCl) and seawater samples (Wittmer~~, Bleicher, Ofner, & Zetzsch, 2015; Wittmer, Bleicher, & Zetzsch~~ et al., 2015a,b) and in laboratory experiments (Mikkelsen et al., 2024). Recently, this process has been ~~demonstrated~~ hypothesized to occur in the atmosphere in a study based on observations from Barbados through the mixing of natural iron-containing dust and sea salt aerosols and is thought to be due to the release of chlorine gas (Cl_2) followed by rapid photolysis (van Herpen et al., 2023). Gorham et al. (2024~~3~~) present the state of the science for moving forward with intentional increase of this mechanism via iron salt aerosol. Meidan et al. (2024) find that the impact of iron varies depending on the region of application. Recent work has investigated the direct release of Cl_2 in a coupled chemistry–climate model and found that at least 90 Tg/yr Cl_2 is needed for Cl increases to outweigh decreases in OH with respect to overall methane loss, and at least 1,250 Tg/yr Cl_2 is needed to decrease the methane lifetime by 50% or more (Li, Meidan, et al., 2023).

Here I simulate in an atmospheric model a variety of methods of atmospheric oxidation enhancement (AOE) of methane via tropospheric OH and tropospheric Cl. I assess their impacts on methane, tropospheric chemistry, other greenhouse gases and ozone-depleting substances, and surface air quality.

2 Methods

I apply the global atmospheric chemical transport model GEOS-Chem (Section 2.1) with modifications (Section 2.2) to simulate atmospheric oxidation enhancement scenarios and their effects. The overall methodology of the study is outlined in Figure S1.

2.1 GEOS-Chem Model

Here I apply the 3D atmospheric chemical transport model GEOS-Chem version 13.2.1. (https://doi.org/10.5281/zenodo.5500717). As it is a chemical transport model, meteorological and climatic processes are not simulated directly. Instead, the model is driven by assimilated offline meteorological fields of the Modern-Era Retrospective Analysis for Research and Applications (Gelaro et al., 2017) from the National Aeronautics and Space Administration/Global Modeling and Assimilation Office. Simulations are performed at 4° latitude × 5° longitude horizontal resolution, with 72 vertical layers from the surface to the mesosphere (up to 80 km) and with active chemistry through the stratosphere (up to 50 km). Simulations are performed for the arbitrary year 2019 following 1 year of initialization (year 2018).

Detailed coupled tropospheric halogen (chlorine, bromine, iodine) chemistry follows Wang et al. (2021) and includes sea salt debromination, acid displacement, and improvements to heterogeneous chemistry on polar stratospheric clouds (Eastham et al., 2014). Online stratospheric chemistry includes heterogeneous ozone depletion chemistry. Carbonaceous aerosol includes black carbon (Wang et al., 2014) and organic aerosol following the "simple" secondary organic aerosol (SOA) scheme (fixed-yield, direct, and irreversible formation) (Pai et al., 2020). Anthropogenic emissions follow the Community Emissions Data System (CEDS) v2 inventory originally developed for the Coupled Model Intercomparison Project Phase 6 (CMIP6) (https://data.pnnl.gov/dataset/CEDS-4-21-21), including particulate iron emitted as a constant fraction of sulfur dioxide (SO_2). The speciation and solubility of iron in GEOS-Chem is discussed in Section 2.2.2.3. Sea salt aerosol emissions over the open ocean are wind- and sea surface temperature–dependent following Jaeglé et al. (2011), and in polar regions include blowing snow (Huang & Jaeglé, 2017). Dust emissions include natural (Fairlie et al., 2007) and anthropogenic dust from the anthropogenic fugitive, combustion, and industrial dust inventory (Philip et al., 2017). Biogenic volatile organic compound emissions are from MEGAN v2.1 (Guenther et al., 2012). All meteorologically dependent emissions are calculated offline at the native model resolution (0.5° × 0.625°) (Weng et al., 2020) and appropriately scaled such that the total emissions are independent of model resolution (Lin et al., 2021). Wet deposition follows Amos et al. (2012) for gases and Liu et al. (2001) for aerosols, with snow and mixed precipitation scavenging from Wang et al. (2014). Dry deposition is a resistance-in-series approach (Wang et al., 1998) with aerosol dry deposition described in Zhang et al. (2001). Ozone deposition to the ocean via reaction with sea surface iodide follows Pound et al. (2020). Planetary boundary layer mixing follows a non-local scheme (as opposed to assuming full mixing) as implemented by Lin and McElroy (2010). The first 2 kilometers contain 14 vertical levels, with gridbox heights increasing from 120m at the surface to 250m by 2km.

Methane concentrations at the surface in GEOS-Chem are a fixed boundary condition based on monthly mean National Oceanic and Atmospheric Administration flask observations, after which methane advects and participates in chemistry (Murray, 2016). Hence, I use the methane feedback factor, which accounts for the feedback of methane on its own loss rate to estimate changes in steady-state methane concentrations. Impacts on steady-state methane concentrations

estimated using fixed boundary conditions along with the methane feedback factor are within 10% of impacts predicted from long (>40 years) simulations reaching equilibrium with fully responsive surface methane fluxes, while significantly reducing the computational cost (Khodayari et al., 2015). Fixed boundary conditions combined with the feedback factor also have been found to have a negligible impact on estimates of the global warming potential of hydrogen accounting for indirect methane feedbacks (Warwick et al., 2023). Here, I first calculate the methane lifetime following the same methods as in Horowitz et al. (2020) from Holmes et al. (2013) and Holmes (2018). Briefly, the partial lifetimes of methane against tropospheric OH and Cl are calculated from the integrated 3D reaction rates. The total methane lifetime includes these two losses, stratospheric loss (assumed 120 years), and uptake to soil (assumed 150 years). Then, the change in steady-state methane concentration is estimated using the feedback factor *f* following Holmes (2018):

$$\Delta[\mathrm{CH_4}] = \left(\left(\frac{\tau_{exp}}{\tau_0}\right)^f - 1\right)[\mathrm{CH_4}]_0 \quad (1)$$

where τ_0 and τ_{exp} are the lifetimes of methane in the standard and atmospheric oxidation enhancement experiments, respectively; $f = 1.34 \pm 0.06$ is the GEOS-Chem methane feedback factor on its loss rate (Holmes et al., 2013); and $[\mathrm{CH_4}]_0$ = 1,866.58 parts per billion (ppb) is the global annual mean surface methane concentration in year 2019 (https://gml.noaa.gov/ccgg/trends_ch4/).

2.2 Model Experiments for Atmospheric Oxidation Enhancement

A summary of simulations is presented in Figure S2. Scenarios are grouped between the dominant intended effect on increasing methane oxidation, either through reaction with OH (OH-based; Section 2.2.1) or Cl (Cl-based; Section 2.2.2). Under these umbrellas are experiments with different compounds emitted (OH or hydrogen peroxide for OH-based, and Cl_2 or particulate iron and/or chloride for Cl-based). All emissions are constant in time except for daytime-only tests (for simplicity, double the 24-hour emissions rate released between 6am and 6pm local time) for several of the hydrogen peroxide emissions scenarios, as marked in Figure S2.

For the remainder of the paper, I will focus on scenarios detailed in Table 1, which produced nonnegligible results. Direct OH release scenarios will be discussed briefly in the context of comparisons with the hydrogen peroxide emissions scenarios that led to comparable impacts. Details on the remaining simulations are included in the supplementary information; see Tables S1 and S2.

Table 1: Details of focus scenarios in the current study.

	Emitted Species	Total Emissions (Tg/yr)	Emissions Location	Emissions Rate at Location of Emissions ($kg/m^2/s$)	Reaction Rate Coefficient
H_2O_2_high	H_2O_2	1.61E7	Globally at surface	1.00E-6	N/A
H_2O_2_mid	H_2O_2	7.4E4	Globally at surface	4.6E-9	N/A
H_2O_2_low	H_2O_2	1,250	Globally at surface	7.7E-11	N/A
Cl_2_ocean	Cl_2	1,250	Oceans	1.10E-10	N/A
Cl_2_BrCl_Br_2	Cl_2 BrCl Br_2	1,193 187 129	Oceans	1.045E-10 1.137E-11 1.64E-11	N/A
Iron	pFe*	565	Oceans	4.97E-11	$d[Cl_2]/dt = \alpha j_{NO2} [Fe^{3+}][Cl^-]S$
Iron_Max	pFe	1,250	Oceans	1.10E-10	
Chloride	Accumulation mode chloride	1,250	Oceans	1.10E-10	
Iron_Chloride	Accumulation mode chloride pFe	1,250 565	Oceans	1.10E-10 4.97E-11	

**pFe is particulate iron.*

2.2.1 Hydroxyl Radical

2.2.1.1 Hydrogen peroxide emission

Hydrogen peroxide photolysis produces two OH radicals, and the emission of hydrogen peroxide has been proposed as a possible method to enhance atmospheric methane oxidation via OH (Wang et al., 2022). For example, there is a patent to deploy hydrogen peroxide towers for this purpose (Bell, 2023). The concurrent production of hydrogen peroxide and release of OH via Fenton-like catalytic processes has also been suggested as a potential technology (Wang et al., 2022).

In this study, I tested four scenarios to investigate the impact if the current global demand of 4.1 Tg/yr H_2O_2 (Research and Markets, 2023) was released additionally (see Figure S2): globally at the surface, only at major point sources of oil and gas emissions determined from the CEDS anthropogenic emissions inventory (0.2% of Earth's area at the 4° × 5°

model resolution) at the surface, 600 m (stack height proposed by the Bell, 2023 patent), and 600 m emitted only during daytime to maximize photolysis. All 4.1 Tg/yr scenarios produced negligible effects on the methane lifetime. The change to 600 m stack height as well as from 24-hour to daytime-only did slightly increase the impact on methane (by <<1%) but still resulted in <0.5 ppb (≤0.03%) decrease in methane. As the spatial resolution is low (4° × 5° or 400–500 km at midlatitudes), this current model study may not address fully whether this method is viable for individual, large point sources of methane. Given the negligible results found here, these scenarios were not investigated further in this study. Another study using the GEOS-Chem model investigated daytime-only 600 m H_2O_2 towers in more detail over North America at a higher spatial resolution (0.5° × 0.625° or ~50 km), and found that even widespread towers at emissions rates 10x higher than what is currently proposed would lead to negligible impact on global methane (Mayhew and Haskins, 2025). This is in part because the fraction of H_2O_2 converted to OH is ~30-60% but is driven by the small fraction of the produced OH that reacts with methane (23% at the most and frequently much less) (Mayhew and Haskins, 2025).

For the remainder of the paper, I will focus on three global hydrogen peroxide emissions scenarios to span a range of impacts on methane and feasibility (H_2O_2_high, H_2O_2_mid, and H_2O_2_low; see Table 1). H_2O_2_low emits the same mass as the Cl_2 experiment (1250 Tg/yr; see Section 2.2.2.1) for comparison purposes. Short-term tests were performed with increasing H_2O_2 emissions to estimate the quantity needed such that methane would decline by at least 50% (leading to H_2O_2_high). All scenarios were emitted at the surface (0 to 12.3 m altitude in GEOS-Chem). In the 4.1 Tg/yr point source tests, impacts increased when the hydrogen peroxide was emitted at 600 m with respect to the surface. It is thus possible that the impacts on methane by these global scenarios could be larger if emitted at 600 m, potentially due to a longer lifetime for H_2O_2 allowing for greater photolysis; this would require further investigation. I also tested H_2O_2_mid and H_2O_2_low with double the 24-hour emissions rate only released during 6am–6pm local time. Daytime-only emissions did increase the impact on methane, with a larger relative effect for the smaller hydrogen peroxide emissions, but the absolute values of methane lifetime and steady-state methane concentrations are within ±1% for the corresponding daytime-only and 24-hour emissions scenarios. Thus, I will focus on results from the 24-hour emissions for the remainder of the paper.

2.2.1.2 OH chemical production

Not all hydrogen peroxide is immediately photolyzed to produce OH and may undergo alternate reactions. Estimates include the previously described GEOS-Chem study which found approximately 30-60% of H_2O_2 on average is photolyzed, but this is highly spatially variable (Mayhew and Haskins, 2025), and a conservative theoretical estimate of 10% based on all potential chemical and physical pathways (Pennacchio et al., 2024). Thus, to examine the direct effects of OH release in the absence of other chemical changes, I introduced a dummy reaction in GEOS-Chem to produce OH from O_2, a species with fixed concentrations in GEOS-Chem (0.2095 mol/mol), from the surface up to 1 km altitude globally (see Table S2 in the supplementary information). OH cannot be advected in GEOS-Chem due to its short lifetime and thus it cannot be emitted directly. I tested two rates, OH_mid and OH_high; OH_high's rate of OH emission is two times higher (see Table S2) to result in similar changes to OH as the hydrogen peroxide simulations (since H_2O_2 photolyzes to produce 2OH). In

reality, OH could be released directly through methods incorporating artificial UV radiation (e.g., Ming et al., 2022) or downdraft energy towers that generate electricity from seawater and sunlight and produce additional OH from ozone due to the water vapor introduced in dry regions (Tao et al., 2023; Wang et al., 2022); these would likely be point sources that are not feasible in the current modeling framework. Given this and the fixed methane boundary conditions, the direct OH results will only be discussed in reference to how air quality impacts change when OH versus hydrogen peroxide is emitted at comparable impacts on methane.

2.2.2 Chlorine

2.2.2.1 Direct Cl_2 emission

In the Cl_2 simulation, Cl_2 is directly emitted across the global oceans at the surface, a total of 1,250 Tg/yr, which is the midrange scenario for methane removal in Li, Meidan et al. (2023) (resulting in 45% reduction in the methane burden in their study). This is approximately 20 times higher than the current total tropospheric source of gas-phase inorganic chlorine in GEOS-Chem (54 Tg/yr; Wang et al., 2021) or the current manufacture of Cl_2 (58 Tg/yr; World Chlorine Council). Emissions of Cl_2 at the surface are more likely to be economically and technologically feasible and will limit the impact of additional chlorine on stratospheric ozone (Li, Meidan, et al., 2023). Cl_2 will then photolyze to produce two Cl atoms, of which approximately 20% will react with ozone instead of methane over the oceans (Li, Meidan, et al., 2023). Table S43 compares the modeling setup of the current study and Li, Meidan et al. (2023), including differences in resolution, year, and halogen chemistry.

2.2.2.2 Bromine contamination

It is not possible to remove 100% of bromide from pure chlorine salts (for example, Sigma-Aldrich S9888 ≥99.0% NaCl specifications include up to 0.01% Br^-; https://www.sigmaaldrich.com/). This could lead to reactive bromine release that would decrease OH in the atmosphere through the destruction of ozone, the primary HO_x (HO_x = OH + HO_2) source (e.g., Horowitz et al., 2020), while unlike Cl it does not also oxidize methane. Here I create a model experiment (Cl_2_BrCl_Br_2) including direct emission of the bromine species Br_2 and BrCl. Wittmer~~, Bleicher, and Zetzsch~~ et al. (2015b) measured the Br versus Cl production rate from artificial sea salt created from a variety of iron-containing artificial seawater or NaCl stock solutions, with the ratio of Br/Cl produced by mass ranging from 0 to a factor of 2.5. Br atom was below the detection limit for the NaCl-based solutions (Wittmer~~, Bleicher, & Zetzsch,~~ et al., 2015b), which may better resemble artificially engineered iron salt aerosol. However, previous work with salt pans found that even when Br atom ~~was~~ concentrations were below the detection limit, bromide impurities in "pure" NaCl (≤ 0.01% Br^-) could lead to Cl atom release due to BrCl formation and photolysis, which would also release Br atoms in equal quantities (Wittmer~~, Bleicher, Ofner, & Zetzsch,~~ et al., 2015a). Here I assume that of the total desired chlorine release (1,250 Tg/yr as in the Cl_2-ocean simulation), 20% of that by mass of bromine is released in equal parts Br_2 and BrCl (resulting in 1193 Tg/yr Cl_2, 187 Tg/yr Br_2, and 129 Tg/yr BrCl). This scenario represents a bounding case if artificial sea salt containing bromine impurities were to be continuously emitted as part of an AOE method. In prior work, increasing the flux of natural sea salt aerosol in GEOS-

Chem led to relative increases in tropospheric-wide reactive bromine that were comparable to that of reactive chlorine (Horowitz et al., 2020). More laboratory studies are needed to understand the potential bromine release from engineered iron salt aerosol.

2.2.2.3 Iron salt aerosol

Here I implement a parameterization of photolytic Cl_2 release from iron-enriched salt aerosol developed by Chen et al. (2024). The production rate of Cl_2 ($d[Cl_2]/dt$: molecules cm^{-3} s^{-1}) is a function of the nitrogen dioxide (NO_2) photolysis frequency (j_{NO2}: s^{-1}), accumulation mode aerosol iron (III) concentration ($[Fe^{3+}]$: mol l^{-1} water, or M), accumulation mode aerosol chloride concentration ($[Cl^-]$: ~~mol l^{-1}~~M), and aerosol surface area concentration (S: μm^2 cm^{-3}), and is scaled by the factor α (=1.4 × 10^5 molecules μm^{-2} M^{-2}) based on experimental results from Wittmer~~, Bleicher, and Zetzsch~~ et al. (2015b) accounting for the volume of the chamber:

$$d[Cl_2]/dt = \alpha j_{NO2}[Fe^{3+}][Cl^-]S \quad (2)$$

This reaction ($Cl^- \rightarrow 0.5Cl_2$) occurs on chloride in accumulation mode ~~chloride~~ sea salt aerosol, which in GEOS-Chem is defined as ≤0.5 μm in diameter. Additional details on the parameterization calculations including α and the chamber volume correction are presented in Text S1 and Table S3 in the Supplementary Information.

Spatiotemporally varying photolysis frequencies (including j_{NO2}) are calculated online in GEOS-Chem using the Fast-JX scheme (Neu et al., 2007) as implemented by Mao et al. (2010) and account for cloud optical depth. In the standard GEOS-Chem model, Fe(III) concentrations are estimated from natural dust up to 1 μm and anthropogenic particulate Fe (pFe) for the Fe(III)-catalyzed SO_2 oxidation chemistry. This assumes that total Fe content from dust is 3.5% of total mass (Taylor & McLennan [1985], consistent with Trapp et al. [2010]), dust iron solubility is 1% (Alexander et al., 2009) while anthropogenic particulate Fe is more soluble at 10% (Shao et al., 2019), and Fe(III) is 10% of total dissolved iron in the daytime (Moffet et al., 2012) and 90% at night. These assumptions are not sufficient to match observations in polluted urban environments in China (Chen et al., 2024). Model evaluation against observations suggests four times higher solubility for both dust and anthropogenic Fe (4% and 40%, respectively) and 67% of total dissolved iron as Fe(III) (Chen et al., 2024). Observed Fe solubility in aerosols over the oceans is highly variable (0.19% to 47.8%) and is influenced by the initial source of the iron (e.g., dust vs. combustion), other chemical components in the aerosol, pH, and relative humidity (Shi et al., 2022). For the iron salt aerosol simulations, I use the Chen et al. (2024) representation of solubility and Fe(III) speciation as a maximum rate of Cl_2 production through this particular parameterization. For consistency with the version of the Chen et al. (2024) mechanism that was evaluated against observations (see Section 3.1.2), I also include this process on fine-mode aerosols only; the chamber experiment on which the mechanism is based used fine mode aerosol (Wittmer et al., 2015b) and the lifetime of smaller particles is longer relative to coarse particles such that iron and chloride have time to mix within the aerosols before being deposited (Moffet et al., 2012, Zhu et al., 2022). The dependence on aerosol surface area concentration, and the impacts of pH and potential suppression of the rate by aerosol sulfate and organics (which are not considered in this mechanism) warrant future study. van Herpen et al. (2023) also parameterized the production of Cl_2 from natural mineral dust–sea spray aerosols. Major differences between Chen et al. (2024) and van Herpen et al. (2023) include

the size of the particles on which this process occurs, the percentage of photoactive iron, and that the Chen et al. (2024) study is based primarily on the Wittmer~~, Bleicher, and Zetzsch~~ et al. (2015b) chamber experiments while van Herpen et al. (2023) follow the Fe(II)–Fe(III) cycling kinetics from Zhu et al. (1993). Differences in the model frameworks are summarized in Table ~~S4~~S5.

First I perform GEOS-Chem simulations with the additional reaction of iron-mediated Cl_2 release from chloride aerosol from Chen et al. (2024) in the absence of any additional emissions to act as a reference point for the atmospheric oxidation enhancement experiments. Then, to release additional Cl_2 from iron salt aerosol, accumulation mode aerosol chloride and particulate iron (pFe) are released over the oceans at the surface in four scenarios to assess the driving factors and compare against the direct Cl_2 scenario. The highest iron addition tested in Wittmer~~, Bleicher, and Zetzsch~~ et al. (2015b) was 13 mol Cl^-/mol Fe^{3+}. Given the assumed solubility of anthropogenic pFe of 40% and Fe(III) speciation fraction of 67% in my GEOS-Chem simulations, a ratio of 3.484 mol Cl^-/mol pFe emitted would lead to Fe(III) ratios at most comparable to the highest iron addition experiments in Wittmer~~, Bleicher, and Zetzsch~~ et al. (2015b). For accumulation mode aerosol chloride emissions of 1,250 Tg (the same mass of total chlorine emissions as the Cl_2 experiment), this is 565 Tg/yr pFe. The experiments here include particulate iron emissions alone (Iron), aerosol chloride emissions alone (Chloride), a combination of both particulate iron and chloride (Iron_Chloride), and particulate iron alone emitted at 1,250 Tg/yr (Iron_Max) as a test case (see Table 1 for details). Iron_Max does not lead to significantly more methane loss than the Iron scenario; hence, it will only be discussed in the context of methane and not with respect to tropospheric chemistry and air quality.

3 Results

3.1 Impacts on Tropospheric Chemistry

3.1.1 Major Tropospheric Oxidants and Reactive Halogens

Table 2 presents the tropospheric burdens of major oxidants, reactive halogen families, and carbon monoxide (CO) for the standard GEOS-Chem simulation and the standard simulation plus the Chen et al. (2024) parameterization, followed by relative percent changes in these burdens for the atmospheric oxidation enhancement model experiments described in Table 1.

Table 2. Percent change in simulated annual mean tropospheric burdens of selected species and chemical families.

	Br_y	Cl_y	I_y	O_3	OH	Cl	NO_x	CO
Standard	20 Gg	2401~~1~~ Gg	12 Gg	338.4 Tg	2145~~5~~ Mg	3138~~8~~ kg	3605~~59~~ Gg	3504~~9~~ Tg
Standard+Chen	20 Gg	241 Gg	12 Gg	337.8 Tg	2145~~5~~ Mg	3433~~3~~ kg	359 Gg	3504~~9~~ Tg

H2O2_high	-121.21%	36.7%	-77.5%	-38.5-38.5%	165.9%165.3	401.7%396.4	8.2%8.3	-46.4%-46.3
H2O2_mid	448.2%	12.3%	-20.36%	-6.0-6.3%	30.3%30	73.8%75.2	-17.1%-17.2	-23.2%-23
H2O2_low	911.60%	0.9%	-1.24%	-0.7-0.8%	2.3%2.3	6.3%6.5	-4.1%	-2.9%-2.8
Cl2	-6.17%	1738%	-42.7%	-24.4%	-27.7%-27.6	2213.62%185.2	-18.7%	52.2%52.1
Cl2_BrCl_Br2	259677%	1689%	-75.24%	-67.1-67.7%	-47.1%-47.6	1869.5%1839.8	-30.6%-31.1	98.6%100.1
Iron*	67.1%	12.01%	-5.35%	-3.4-3.5%	-2.1%-2.2	169.4%179.3	-2.5%-2.6	3.3%
Chloride*	465.95%	1114.6%	-8.76%	-5.6-5.5%	-3.9%	178.6%180.9	-3.5%	4.2%
Iron_Chloride*	432.47%	11413 9%	-17.23%	-10.6-10.7%	-8.6%	658.0%680.8	-9.2%-9.3	13.5%

Note: Percent change in annual mean tropospheric burdens for model experiments (described in Table 1) are relative to the standard version (* = relative to standard + Chen et al., 2024). Br_y, Cl_y, and I_y follow definitions in Wang et al. (2021); NO_x =NO + NO_2. See also Section 2.1.

Previous work on an intermodel comparison of atmospheric chemistry and climate models from the Atmospheric Chemistry and Climate Model Intercomparison Project found that changes in global mean OH between models and within a given model are more a function of the relative loss of reactive nitrogen versus reactive carbon than the emissions of reactive nitrogen versus carbon, as it matters how much of the loss of these species is due to OH versus other processes (Murray et al., 2021). The loss of reactive carbon is a function of a given model's chemical mechanism and structure (Murray et al., 2021). The GEOS-Chem model version used in this study (13.2.1) is several generations ahead of that used in Murray et al. (2021) (version 9-01-03), with a number of changes in reactive nitrogen chemistry including aerosol uptake and recycling of isoprene nitrates (e.g., Fisher et al., 2016, 2018; Holmes et al., 2019; McDuffie et al., 2018) that have been shown to impact the tropospheric OH burden by up to 12%. The representation of nitrogen oxides (NO_x) loss thus can lead to uncertainty in the simulated OH burden, but it is not clear if this would be a consistent bias across all model experiments in the current study and thus negligible when considering relative changes.

As expected, the hydrogen peroxide experiments all increase tropospheric OH due to photolysis of the additional hydrogen peroxide. OH does not increase proportionally to the increase in hydrogen peroxide emissions across experiments and indicates a reduction in the effectiveness of additional emissions at higher levels of hydrogen peroxide. A >200-fold

increase in hydrogen peroxide emissions from H_2O_2_mid to H_2O_2_high leads to a 5.5-fold increase in the change of OH; a 60-fold increase in hydrogen peroxide emissions from H_2O_2_low to H_2O_2_mid leads to a 13-fold increase in the change of OH (see Table 2). The increases in OH drive reductions in tropospheric CO seen in these experiments, as OH is the main oxidant of CO. The reductions in CO are nearly proportional to the OH increases in the H_2O_2_low and H_2O_2_mid scenarios; however, in the extreme H_2O_2_high scenario, the CO decrease is much lower than expected from the OH increase (see Table 2). This is likely due to the much larger increase in Cl atom in the H_2O_2_high experiment, leading to additional production of CO from Cl reactions with formaldehyde and organochlorines (see Table S6 in the SI). In all of the hydrogen peroxide experiments, Cl atom increases. Increased HO_x (= OH + HO_2, which cycle rapidly between each other) leads to increased release of chlorine from sea salt aerosol and organohalogens (see Table S6 in the SI and Wang et al., 2021), increasing the total Cl_y burden. Within each experiment, the longer-lived reservoir species hydrogen chloride (HCl) contributes the largest mass to the total Cl_y burden. ~~In addition~~However, relative to the standard simulation the partitioning of gas-phase Cl_y shifts away from ~~the longer-lived reservoir species~~ ~~hydrogen chloride (~~HCl~~)~~ toward chlorine hydroxide (HOCl), Cl_2, and Cl, such that the relative increase in Cl atom is greater than the relative increase in total Cl_y ~~in~~ for each experiment. This is due to the complex interplay of cross-reactions between fast-cycling HO_x and chlorine radicals as well as across their longer-lived reservoir species. For example, in addition to the reactions in Table S6 which are sources of gas-phase Cl_y rather than cycling between species, OH can react with HCl to produce Cl atom.

Cl-based experiments decrease tropospheric OH due to the destruction of ozone by the additional Cl, as ozone provides the main source of tropospheric OH. Tropospheric CO increases in the chlorine-based experiments, partially due to the decrease in OH as well as the additional production of CO from reactions of formaldehyde and organochlorines with Cl atom. The Cl_2, Chloride, and Iron_Chloride experiments have the same amount of total chlorine emissions (see Table 1) but vastly different effectiveness at increasing the Cl atom concentration due to the emitted species (gas-phase Cl_2 or particulate chloride) having different reactivities and reactions. The Chloride and Iron_Chloride experiments, where particulate accumulation mode chloride was emitted, have 64 to 66~~5~~% as much of an increase in total gas-phase Cl_y burden relative to the Cl_2 experiment where gas-phase Cl_2 was emitted (see Table 2). However, only 8% (Chloride only) to 30~~1~~% (Iron_Chloride) of the increase in Cl atom seen in the Cl_2 experiment is realized. This is because the vast majority of the increase in Cl_y burden in these experiments is due to HCl, shifting Cl_y away from more reactive species. As in the hydrogen peroxide experiments, HCl still remains the dominant component of Cl_y. The release of Cl_2 is iron-limited, as the addition of particulate iron emissions with the same amount of chloride (from Chloride to Iron_Chloride) leads to a nine-fold increase in Cl_2 and a three-fold increase in Cl (see Table S7).

In the Cl_2 and Cl_2_BrCl_Br_2 experiments, Cl_y partitioning is shifted away from HCl to Cl_2 and Cl. Thus, the relative increase in Cl atom is even greater than the relative increase in total tropospheric Cl_y (see Table 2). In Li, Meidan et al. (2023), 1,250 Tg/yr Cl_2 le~~a~~d to a 30-fold increase in the tropospheric Cl burden; these emissions in our shorter-term modeling study led to a 23-fold increase in the Cl_2-only case and a 20~~19~~-fold increase in the Cl_2_BrCl_Br_2 case (where 1250 Tg/yr of total chlorine was split between 1193 Tg/yr as Cl_2 and the remainder as BrCl). In GEOS-Chem, the only fate of

BrCl is photolysis to produce Cl atom. Hence, the smaller impact of the Cl_2_BrCl_Br_2 scenario on total tropospheric Cl atom is due to the increases in Br_y in this experiment (see Table 2) and the coupled chemistry of Br_y species with Cl_y cycling. ~~This may be due to differences in the reactive halogen reactions and rate coefficients between the model used here versus in Li, Meidan et al. (2023) and the timescale of the study (see Table S3).~~

All experiments decrease the tropospheric ozone burden (see Table 2), with implications for ozone radiative forcing. All experiments have increased Cl atom concentrations, which can destroy ozone. H_2O_2_low, H_2O_2_mid, and all chlorine experiments except Cl_2 also have increased Br_y burdens, which can lead to additional ozone loss via reactive bromine. Increases in OH in the hydrogen peroxide experiments could lead to increased sources of Br_y from sea salt and organohalogens (see Table S6 and Wang et al., 2021). In the H_2O_2_low, H_2O_2_mid, and chlorine experiments, part of the change in ozone is also due to reductions in NO_x that lead to reduced ozone production. This is consistent with previous work which found more active halogen chemistry leads to reductions in NO_x (e.g., due to hydrolysis of halogen nitrates) (e.g., Wang et al., 2019, 2021; Sherwen et al., 2016b; Horowitz et al., 2020). The increases in Br_y and decreases in NO_x, which became larger as hydrogen peroxide emissions increase from H_2O_2_low to H_2O_2_mid, flip sign once hydrogen peroxide emissions become particularly extreme in the H_2O_2_high scenario. Thus in the H_2O_2_high case, the ozone loss is likely dominated by the large increase in Cl atom (see Table 2).

As seen in Horowitz et al. (2020), the decreases in ozone drive decreases in tropospheric I_y in all experiments, as ozone reactions with sea surface iodide are the dominant source of tropospheric I_y (Wang et al., 2021). The greatest impacts on ozone are in the Cl_2_BrCl_Br_2 experiment, which included bromine release to represent bromide contamination (see Table 1). The 20% additional mass released as bromine (Br_2 and BrCl, which both photolyze to release Br atom) led to a much larger than 20% additional reduction in ozone over the Cl_2-only experiment (factor of 2.758 higher) and hence OH (factor of 1.702 higher) (see Table 2). While 20% is likely an overestimate of the bromide content of engineered aerosol, it is well within the range reported from natural seawater salt experiments catalyzed by iron (Wittmer~~, Bleicher, & Zetzsch,~~ et al., 2015b) and suggests that even a small perturbation in bromine could have a much larger impact on OH.

The OH_mid and OH_high scenarios lead to 51% to 94% increases in OH, respectively ~~that are larger than the H_2O_2_mid experiment but smaller than H_2O_2_high~~ (see Table ~~S5~~S8). ~~The behaviors of the other tropospheric species in Table 2 are all similar to the hydrogen peroxide experiments, except for CO (decrease is less than expected given OH increase) and Cl (hydrogen peroxide experiments have a relative increase in Cl that exceeds that of the relative increase in OH; for OH experiments it is less)~~Despite a much larger increase in OH in OH_high than in OH_mid, the decrease in CO is only 5% larger. The OH experiments' results for CO are less reliable than the H_2O_2 experiments as the OH increase is limited to the lower 1 km where it is released. (OH is not transported in the model; hydrogen peroxide is.) In this region, methane levels remain high due to the surface boundary condition and long lifetime against reaction with OH; as CO is reacted away by the additional OH, its loss rate slows down due to its shorter lifetime and fully responsive concentrations at the surface.

3.1.2 Impacts on Methane

Figure 1 (top panel) summarizes the impacts on the overall methane lifetime, the impacts on the methane lifetime with respect to tropospheric OH, and the percent of Cl atom contributing to total chemical loss in the troposphere for each of the experiments in Table 1 and the standard model. Figure 1 (bottom panel) shows the resulting relative change in steady-state methane concentrations estimated with the methods described in Section 2.1.

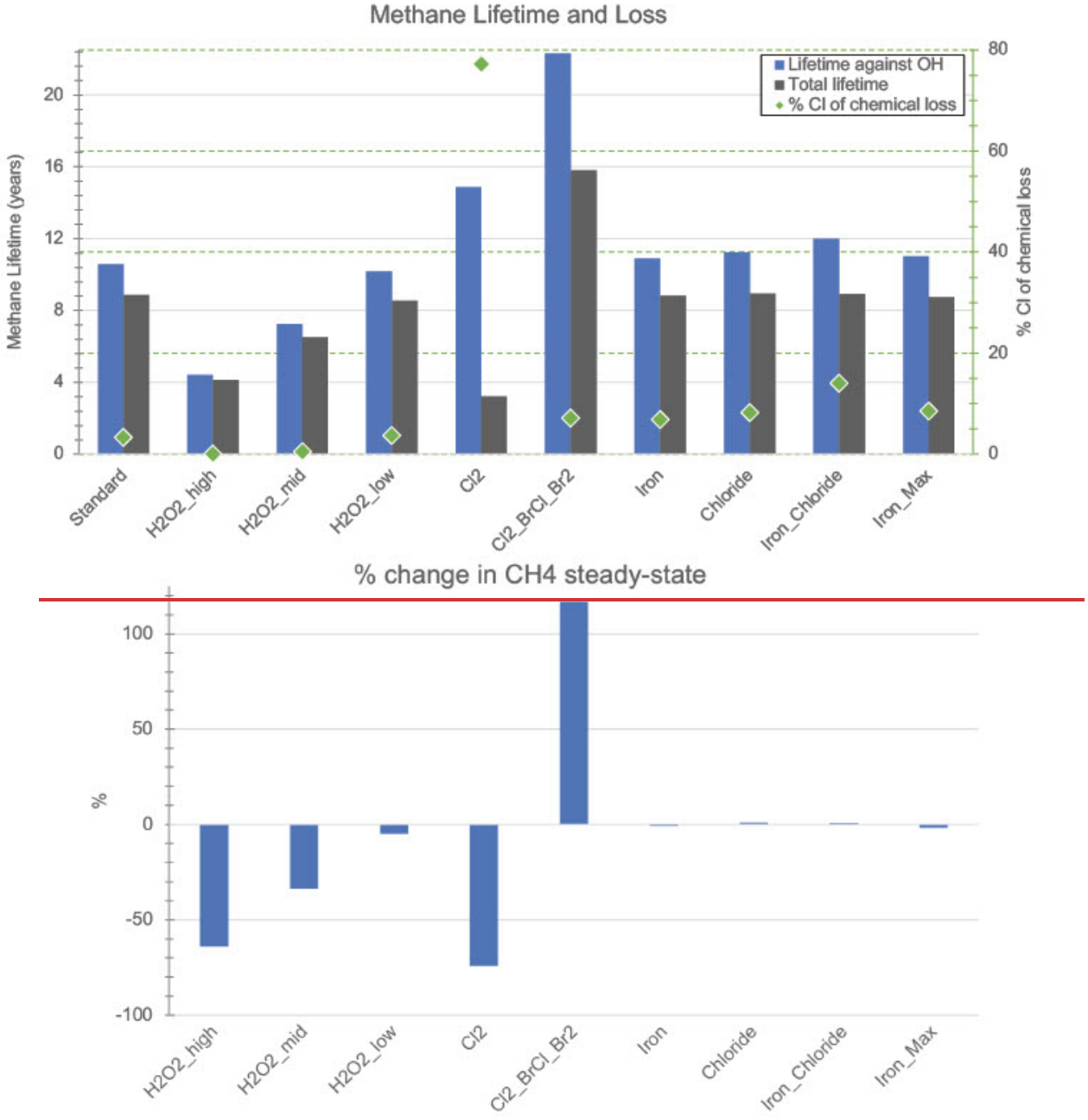

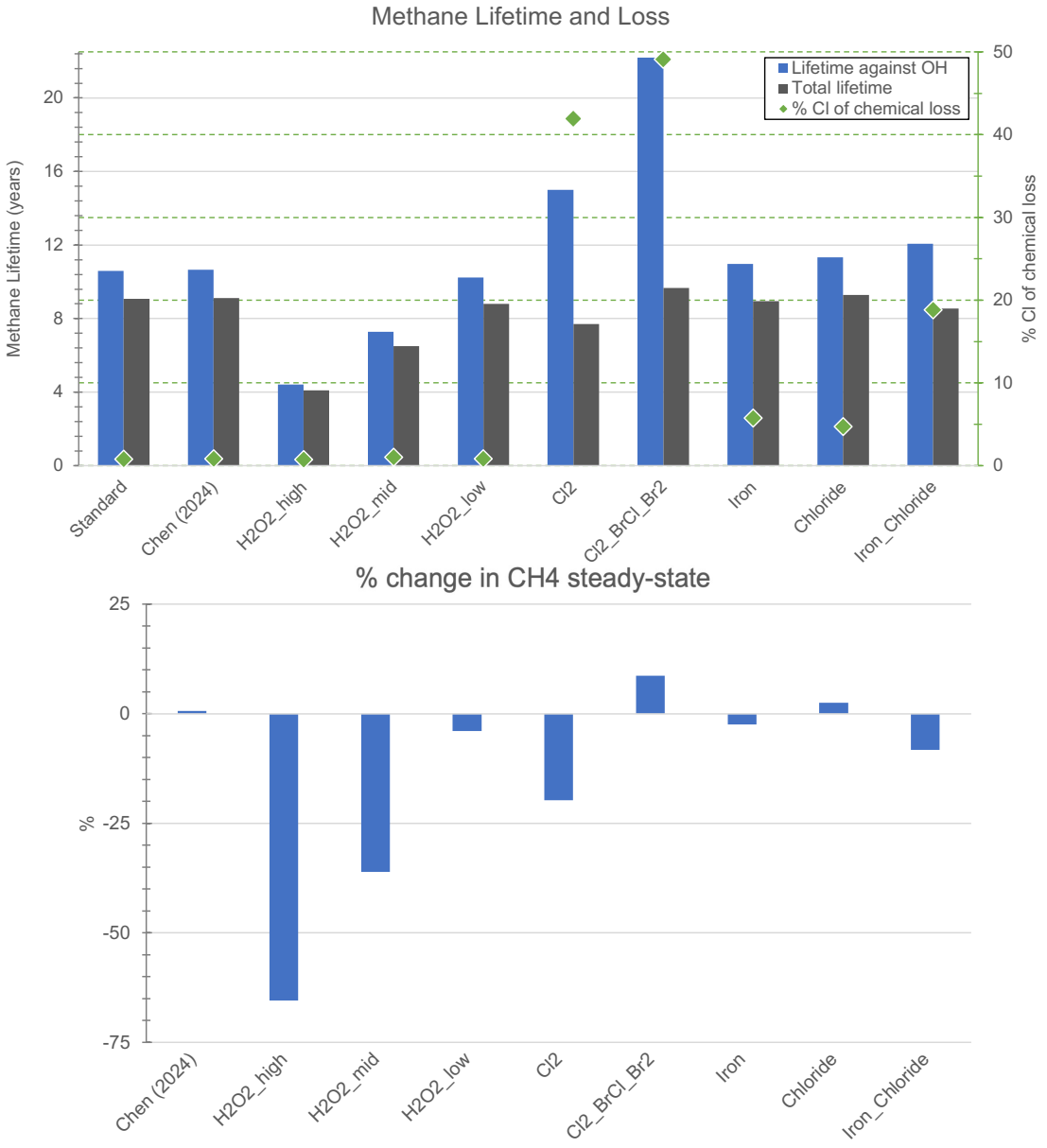

Figure 1: Top panel: total methane lifetime (gray bars) and methane lifetime against oxidation by OH (blue bars), overlaid by the percent of chemical loss contributed by Cl atom (green diamonds, right-hand y-axis). Bottom panel: estimated relative percent change in steady-state methane concentration.

Studies suggest that the present role of chlorine in tropospheric methane oxidation is 0.23~~1~~–5% based on constraints from isotopic observations (Allan et al., 2007; Gromov et al., 2018; Platt et al., 2004) and atmospheric modeling studies focused on chlorine chemistry (e.g., Hossaini et al., 2016; Wang et al., 2019, 2021). The standard version of GEOS-Chem

4used here is consistent with these constraints at ~~3.3~~0.8%, which gives confidence to the simulation of atomic chlorine and its reaction with methane.

Although the H_2O_2_high experiment had ~~the largest increase in tropospheric OH~~more than 5x greater increase in tropospheric OH than that of H_2O_2_mid (see Table 2), the methane lifetime against OH decreases by less than a factor of 2 (Figure 1). The efficacy of H_2O_2 with respect to oxidizing methane via tropospheric OH and decreasing steady-state methane concentrations decreases with increasing emissions (see Figure S3). There is a larger difference between the scenarios for the change in steady-state methane, which also accounts for changes in the lifetime against tropospheric Cl. While all H_2O_2 experiments also lead to increased Cl atom (see Table 2), H_2O_2_low is most efficient at also decreasing the methane lifetime against oxidation by tropospheric Cl for its smaller level of emissions (Figure S3). ~~the chemical loss through the Cl pathway is shut down (Figure 1), leading to a smaller impact on the methane lifetime relative to the comparable OH scenarios (not shown).~~ Significant methane reductions for the hydrogen peroxide scenarios (>5%) require more than 1,250 Tg/yr emissions (H_2O_2_low).

For the same annual emissions of Cl_2 (1,250 Tg/yr) as in Li, Meidan et al. (2023), I find ~~similarly large~~slightly smaller decreases in the methane lifetime (here ~~-67~~-15% vs. 50%) and methane concentrations (here ~~-74~~20% at steady-state vs. –45% in year 2050) despite vastly different modeling frameworks (Table S4). ~~While the tropospheric burden of Cl increases more in~~ Li, Meidan et al. (2023) finds a larger increase in the tropospheric burden of Cl atom, as described in the previous section (factor of 30 vs. factor of 23), ~~I find a~~and a larger percent of methane chemical loss due to tropospheric chlorine (~~77% vs.~~ 60% vs. 41%). ~~This may be due to d~~Differences in our results may be due to differences in the vertical distribution of Cl as well as the meteorology between the two models, as the Cl + CH_4 reaction is temperature-dependent (see Table S6) and the impacts of local changes in the reaction rate on the global methane lifetime are weighted by air-density~~ dependent~~. The vertical distribution of Cl in the two models is not only impacted by the halogen chemical mechanism (see Table ~~S3~~S4); in GEOS-Chem, an improved representation of entrainment-limited uptake in clouds and ice cloud particle properties for cloud heterogeneous chemistry leads to significant increases in reactive chlorine, particularly in the upper troposphere where reaction rates are decreased due to low temperatures (Table S6), due to changes in HCl-ClO_x (chlorine oxides) cycling (Holmes et al., 2019). Other differences that could impact the results are the increase in methane emissions in Li, Meidan et al. (2023) following the representative concentration pathway 8.5 scenario, and the shorter simulation period in our study (see Table ~~S3~~S4). Bromine contamination of 20% more than reverses the gains seen in the Cl_2 case, as the Cl_2_BrCl_Br_2 case has an increase in steady-state methane concentrations of ~~117~~8.7% (see Figure 1).

Figures 2 and S4 show the change in annual mean Cl_2 and Cl atom concentrations at the surface and zonally averaged through 20km, respectively, from adding the Chen et al. (2024) mechanism for Cl_2 production from aerosol iron photochemistry. The absolute increase in surface [Cl] (Figure 2) is largest over the North Atlantic ocean, with the largest relative increases over China reaching a factor of 3 (204%). In Chen et al. (2024), simulations were performed for December 9 - 31, 2017 over North China at 16 times higher spatial resolution (0.25° latitude × 0.3125° longitude) than this study (4° × 5°). They also added high-resolution anthropogenic fine-mode aerosol Cl^- emissions in China from Fu et al. (2018) which are

not included here and would further increase Cl_2 production through their mechanism (see equation 2). They found a maximum increase in [Cl] in an individual model gridbox of a factor of 20 to 40 which is consistent with the increased model horizontal resolution relative to my study.

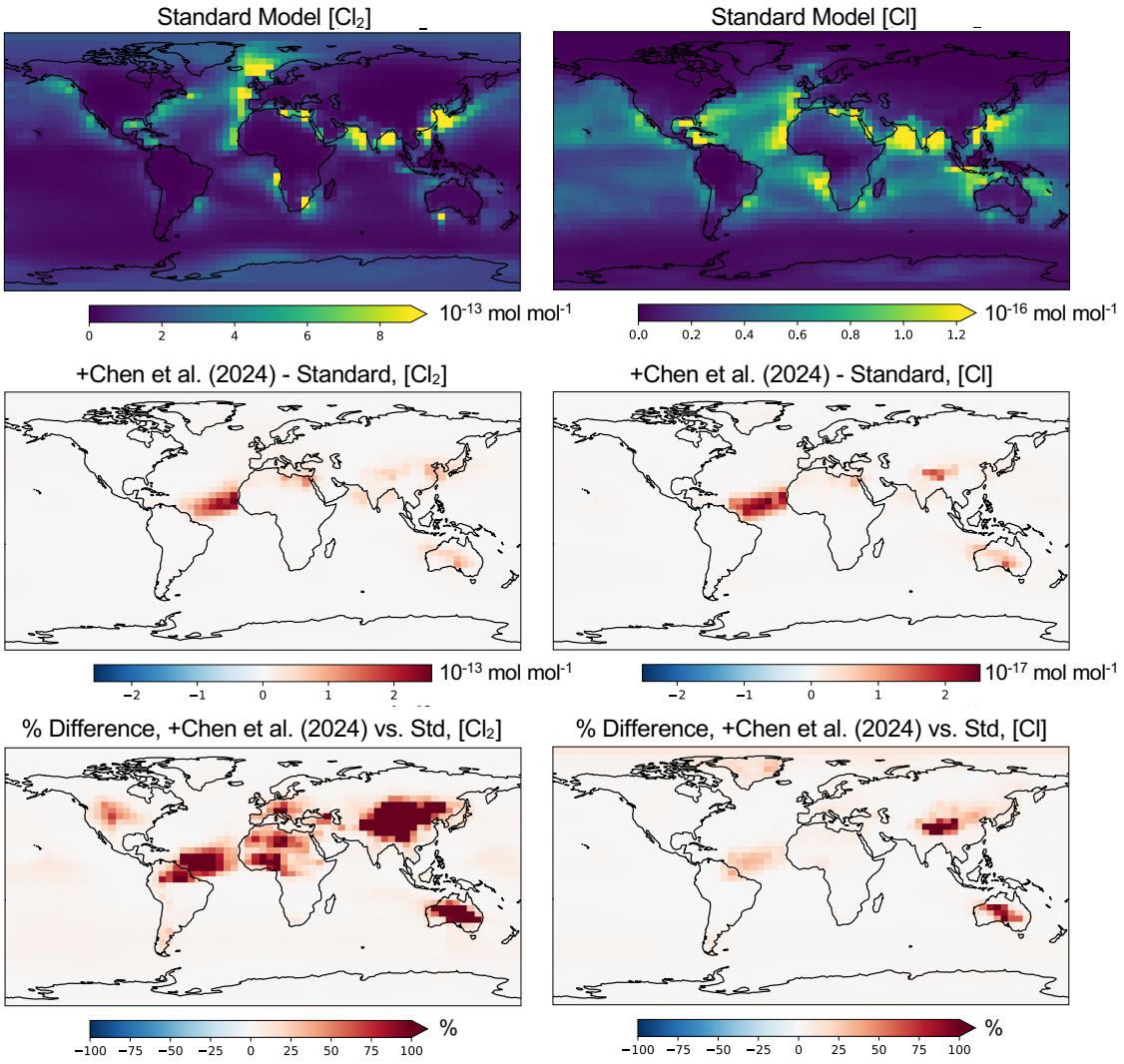

Figure 2: Impacts of adding natural Cl_2 emissions from the Chen et al. (2024) parameterization on simulated year 2019 annual mean surface-level concentrations of Cl_2 (left panels) and Cl (right panels). The top row is the standard model concentrations (mol mol^{-1}), with the second and third rows containing the absolute difference in mol mol^{-1} and relative difference in percent, respectively, from adding the Chen et al. (2024) mechanism.

van Herpen et al. (2023) found that including their parameterization of Cl_2 release from mineral dust–sea spray aerosol (without any additional emissions) led to an increase in methane loss via the Cl atom of ~20%, although the overall global methane loss was decreased slightly due to a reduction in methane loss via reaction with OH. Here I find an increase in the tropospheric burden of Cl atom of 9.4~~–5~~% (see Table 2) when the Chen et al. (2024) parameterization is included (without any additional emissions), ~~but this only~~which translates to an increase of 5.4~~0.2~~% in the methane loss via Cl atom. While van Herpen et al. (2023) do not report global changes in chlorine burdens, they find that total inorganic chlorine production is increased by 41%. This led to a change in –0.7% in the tropospheric ozone burden after including Cl_2 release from natural iron salt aerosol (van Herpen et al., 2023), while I find a change of –0.18~~07~~% in the tropospheric ozone burden when I include the Chen et al. (2024) parameterization. Thus, it is likely that the two parameterizations (see Table ~~S4~~S5) result in Cl_2 production rates that are up to 4~~10~~ times higher in van Herpen et al. (2023).~~-~~ In the zonal mean, increases in [Cl_2] and [Cl] from including the Chen et al. (2024) production mechanism are largest aloft (Figure S4). van Herpen et al. (2023) limited their mechanism to the lower troposphere. Hence, differences in the vertical distributions of changes in chlorine vs. concentrations of ozone and methane in the two parameterizations may further contribute to the differences in impacts. The Chen et al. (2024) mechanism was evaluated directly against hourly observations of gas-phase Cl_2 in Wangdu, China, as well as key parameters including aerosol [Cl^-], aerosol total iron, j_{NO2}, and aerosol surface area (see equation 2). GEOS-Chem also captured the variability and magnitude of daily total Fe and Cl^- concentrations in fine-mode aerosol collected from 29 sites across North China, and slightly underestimated the observed solubility of aerosol Fe which was sampled at two sites, during the intensive study period at Wangdu (Chen et al., 2024). While adding the mechanism greatly improved the model performance of [Cl_2] at Wangdu, increasing simulated concentrations by a factor of 28 to 48, model concentrations remained underestimated. Chen et al. (2024) hypothesized this may be due to overestimated aerosol water in the model's thermodynamic module and thus underestimated aqueous-phase [Cl^-] and [Fe^{3+}]. Low aerosol water content at high altitudes and hence high aqueous concentrations may explain the increases aloft seen in Figure S4. It is outside of the scope of this paper to address uncertainties in the parameterization at higher altitudes.

~~With the parametrization used in this study, iron salt aerosol cannot produce enough chlorine to overcome the decrease in methane loss via the OH channel. Changes in steady-state methane for iron salt scenarios are < ± 2% (see Figure 1).~~ Figure 3 shows the annual mean change in Cl_2 and Cl atom concentrations in the Iron experiment (see Table 1) relative to the model with the Chen et al. (2024) mechanism alone, averaged zonally through 20km altitude. Here, zonal mean increases in [Cl_2] and [Cl] due to iron emissions are largest near the surface (much greater than 400%, up to 60,000%) where emissions are added, unlike when the Chen et al. (2024) parameterization is included in the absence of additional surface emissions (Figure S4). Figures 3 and S4 show that the additional release of Cl_2 due to natural or emitted iron leads to changes in Cl_2 and Cl that have differing spatial patterns and magnitudes in the annual mean due to physical and chemical processing. Tropospheric-wide differences between changes in Cl_2 and changes in Cl (see Table S7) are minor from adding the Chen et al. (2024) parameterization alone or in the Chloride experiment, but diverge most in experiments where iron

emissions are added (Iron and Iron_Chloride). There, the relative increase in Cl_2 is 4 to 6.5 times greater than what is realized for Cl (Table S7).

With the parametrization used in this study, iron salt aerosol can lead to changes in steady-state methane of -8.3% to +2.5% depending on the emissions employed and their relative effects on Cl vs. OH (see Figure 1). ~~While t~~The Iron experiment led to a ~~very~~ small decrease in steady-state methane (–2.5~~0.8~~%) from a tropospheric-wide factor of 2.7~~8~~ increase in Cl atom (see Table S7).~~,~~ T~~t~~he Iron_Chloride experiment led to a ~~small~~ larger de~~in~~crease in steady-state methane (~~+0.7~~ -8.3%) ~~in spite of~~ due to a larger 7.6~~8~~-fold increase in Cl atom burden, despite ~~due to~~ a much larger reduction in OH (-8.6% vs. -2.1%; see Table 2 and Table S7). For ~~the same~~a similar ~~2.8-fold~~ increase in Cl atom burden, emitting chloride (Chloride, 2.8-fold increase in Cl) instead of iron aerosol (Iron, 2.7-fold increase in Cl) ~~similarly~~ led to a larger decrease in OH (-3.9% vs. -2.1%; see Table 2) and hence net increase in methane (+2.5~~0.8~~%). Li, Meidan et al. (2023) found that a 2.8-fold increase in Cl burden (from 88 Tg/yr gas-phase Cl_2 emission) was insufficient to decrease methane, while a 7.9-fold increase in Cl burden (from 313 Tg/yr gas-phase Cl_2 emissions) overcame the OH competition and led to a decrease in methane concentrations by about 6% after 10 years (Li, Meidan, et al., 2023). This suggests that the threshold of additional chlorine needed to overcome the OH limitation depends on what is emitted and the background chemistry in the model employed.

Here I find that emitting sea salt chloride ~~instead of or~~ along with particulate iron ~~worsens~~ increases methane ~~outcomes~~loss. This is a function of the formulation of the Chen et al. (2024) mechanism, which occurs on sea salt chloride aerosol and increases with increasing [Cl^-] concentrations (see Section 2.2.2.3 and Equation 2). Artificial chloride aerosol emissions in addition to the particulate iron emissions can replenish the sea salt chloride that was converted to Cl_2 and increase aerosol [Cl^-] concentrations, leading to greater overall production of Cl_2 (see Table S7).

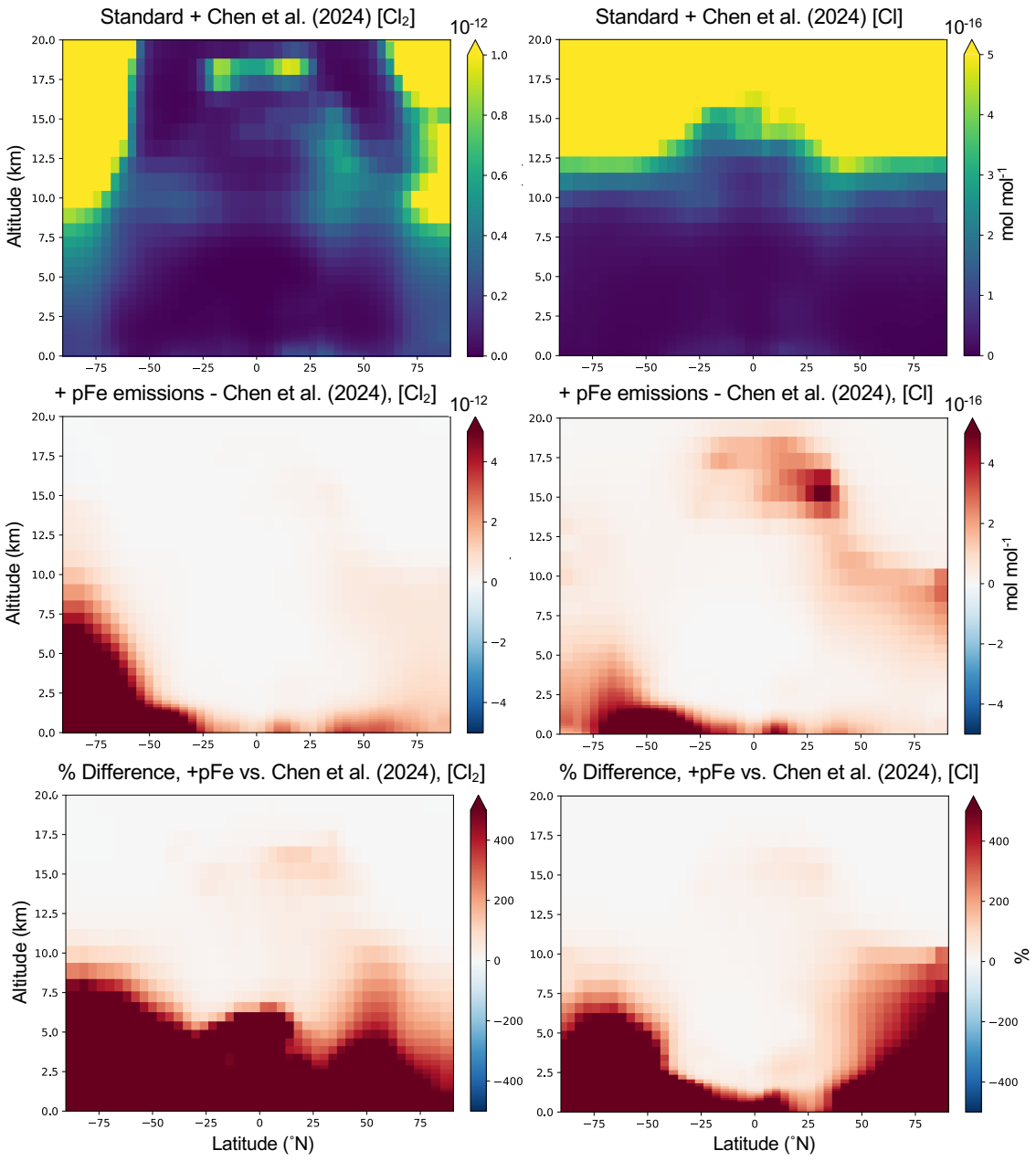

Figure 3: Impacts of adding surface pFe emissions (Iron experiment in Table 1) on simulated year 2019 zonal, annual mean concentrations of Cl_2 (left panels) and Cl (right panels) up to 20km altitude. The top row is modeled concentrations in mol mol^{-1} with the Chen et al. (2024) parameterization alone, with the second and third rows containing the absolute difference in mol mol^{-1} and relative difference in percent, respectively, after pFe emissions are added to the surface layer in this simulation.

The iron emissions needed to decrease methane are also uncertain and sensitive to the mechanism and rate of chlorine release from iron salt aerosol. The Iron and Iron_Chloride scenarios presented here have 565 Tg/yr iron emissions (see Table 1) leading to a decrease in steady-state methane of 2.5% to 8.3%. In a Community Earth System Model (CESM) study using the van Herpen et al. (2023) parameterization for chlorine release, additional iron emissions of 200 Tg/yr (which increased Cl_2 production by ~850 to 930 Tg/yr depending on the region of emission) lead to a ~20% decrease in global methane concentrations after 10 years (Meidan et al., 2024). This study found that a threshold of at least 6 Tg/yr of iron was needed in the most idealized setup to avoid increasing methane, though larger emissions of >60 Tg/yr of iron may be needed for significant methane reductions.

Here, the methane loss in the Iron_Chloride scenario decreases in the tropical and southern hemisphere's free troposphere, with increases in methane loss rates limited mostly to the surface and some regions of the upper troposphere. There may also be a reduction in Cl_2 production from chloride via other reactions with OH and chlorine nitrate ($ClNO_3$) due to reductions in tropospheric OH and NO_x; thus, the representation of competing heterogeneous halogen chemical reactions may play a role in the predicted effectiveness of iron salt aerosol. Additional laboratory experiments and field observations are needed to constrain this process in natural and engineered aerosol mixtures.

Overall, OH-based scenarios and gas-phase emission of Cl_2 lead to significant decreases in steady-state methane but require extremely large emissions. Cl_2 is much more effective at reducing methane (–2077%) than hydrogen peroxide (–45%) for the same level of emission (1,250 Tg/yr). There are uncertainties in the exact impact on methane of a given amount of Cl_2 emission (e.g., in this study vs. Li, Meidan, et al., 2023) due to a variety of factors including the representation of complex reactive halogen chemistry. Despite this, the large methane lifetime and methane concentration reductions from 1,250 Tg/yr of gas-phase Cl_2 emissions presented here are qualitatively similar to those of Li, Meidan et al. (2023). In contrast, by using a different chlorine release mechanism from iron salt aerosol from Chen et al. (2024) and a different atmospheric model, I find that no significant reductions in methane for even larger iron emissions (565 Tg/yr) than those used in Meidan et al. (2024) (200 Tg/yr) lead to a smaller decrease in methane (-2.5% at steady-state vs. -20% after 10 years). The mechanism of Cl_2 emission, whether this would also release bromine, and how fast the release from iron salt aerosol is will affect whether this method would decrease or increase steady-state methane.

3.1.3 Impacts on Other Climate Forcers and Ozone-Depleting Substances

GEOS-Chem simulates additional greenhouse gases and ozone-depleting substances including nitrous oxide (N_2O), halons (three species), hydrochlorofluorocarbons (HCFCs; four species), chlorofluorocarbons (CFCs; five species), and other halomethanes (12 species, e.g., chloromethane, methyl bromide, chloroform). I examined the changes in tropospheric and stratospheric burdens of each. Due to the short simulation length of 1 year following 1 year of initialization, I focus here only on short-lived species (lifetimes <6 months). As our simulation is performed for only 1 year following 1 year of initialization, stratospheric changes do not represent the long-term impact of atmospheric oxidation enhancement of methane due to the long lifetime of air in the stratosphere. At the same time, stratospheric transport and chemistry in GEOS-Chem

~~previously have been evaluated to perform well for stratospheric applications. Earlier versions of GEOS-Chem simulations conducted at the same horizontal and vertical resolution as the current study have shown that age of air at 20 km altitude for all latitudes is within ±6 months of that observed (Eastham et al., 2022), and performs well against in-situ and satellite observations of stratospheric ozone depletion, tracer-tracer correlations, and lifetime of long-lived gases in the stratosphere (Eastham et al., 2014).~~

Details of changes in tropospheric ~~and stratospheric~~ burdens (~~from~~ accounting for the temporally and spatially varying tropopause ~~up to 50 km~~) for selected short-lived species with significant impacts from the AOE experiments are shown in Table~~s~~ S6 ~~and S7~~. ~~For CFCs, halons, N_2O, and most halomethanes, impacts are negligible. Tropospheric burdens of HCFC-123 decrease in the hydrogen peroxide based scenarios and increase in the Cl-based scenarios. Bromide contamination of 20% in the Cl_2_BrCl_Br_2 experiment more than doubles the increase in HCFC-123 relative to the Cl_2 only experiment. HCFC-123 has a 100-year global warming potential of 90.4 (Smith et al., 2021) and is a class-II ozone-depleting substance. Changes in the stratospheric abundance of HCFC-123 are, however, negligible.~~ Of the ~~remaining~~ short-lived halomethanes, bromoform ($CHBr_3$) and dibromomethane (CH_2Br_2) have the largest tropospheric-wide ~~changes in the troposphere and stratosphere~~, with decreases in the hydrogen peroxide–based experiments and increases in the Cl-based experiments. Dichloromethane and chloroform follow the same pattern ~~in the troposphere and stratosphere~~, but changes are smaller overall. For dibromomethane, dichloromethane, and chloroform, the addition of bromine in the Cl_2_BrCl_Br_2 experiment ~~again~~ leads to larger increases relative to Cl_2 only. These short-lived gases could contribute to ozone depletion in the stratosphere and are not regulated by the Montreal Protocol (e.g., Hossaini et al., 2017). Iodine-containing halomethane tropospheric ~~and stratospheric~~ burdens decrease across all experiments due to the reduction in overall I_y (Section 3.1.1), with the largest decreases seen for methyl iodide (CH_3I), which is not thought to contribute to stratospheric ozone loss (Zhang et al., 2020). ~~Li, Meidan et al. (2023) found increases in stratospheric Cl and thus stratospheric ozone loss from the release of Cl_2 for AOE of methane. (In their study, the stratosphere was up to 40 km.) In this study, stratospheric chlorine up to 50 km is negligibly affected in the hydrogen peroxide based experiments with a decrease of −1.5 to −3.1% in the Cl-based experiments. This difference may reflect the short duration of the simulations performed here (1 year vs. 30 years). Overall, in this study, stratospheric ozone changes negligibly in all experiments except in the Cl_2_BrCl_Br_2 scenario, where the stratospheric ozone burden decreases by −7.8%.~~ The shortest-lived HCFC simulated by GEOS-Chem is HCFC-123 (atmospheric lifetime 1.3 years). One year of AOE leads to large changes in its tropospheric burden, with decreases in the hydrogen peroxide–based scenarios (up to -74%) and increases in the Cl-based scenarios (up to 63%). As HCFC-123 has a 100-year global warming potential of 90.4 (Smith et al., 2021) and is a class-II ozone-depleting substance, longer-term simulations are needed to fully quantify the climate impact of AOE.

Across all experiments except Chloride, tropospheric inorganic aerosol increases (see Table S9~~6~~) due to the increase in tropospheric sulfate and ammonium, partially offset by decreases in tropospheric nitrate burdens. This is likely due to the HOCl/HOBr+S(IV) pathways that produce sulfate (Wang et al., 2021), as Br_y and Cl_y both increase in nearly all experiments. This is a departure from Li, Meidan et al. (2023), who found decreases in sulfate of ~10% from 1,250 Tg/yr Cl_2

emissions. This difference may reflect the coupled halogen-sulfate chemistry in GEOS-Chem (Chen et al., 2017; Wang et al., 2021) that does not appear to be included in the CESM chemical mechanism (see Table ~~S3~~S4). For the hydrogen peroxide experiments, increased hydrogen peroxide and OH will also increase the oxidation of SO_2 to sulfate in the aqueous and gas phases, respectively. For the Iron and Iron_Chloride experiments, sulfate may also increase due to the Fe(III)-catalyzed pathway (Alexander et al., 2009). Partitioning of ammonium and nitrate aerosol is determined by the thermodynamic model ISORROPIA-2 in GEOS-Chem (see Section 2.1). Thus, ammonium likely concurrently increases to neutralize the excess sulfate in all experiments. For the Chloride experiment, decreases in nitrate and sulfate are nearly exactly offset by increases in ammonium. Nitrate is likely reduced due to reductions in NO_x in most experiments (see Table 2) and is influenced by the change in gas-particle partitioning due to increased sulfate production. Increases in the tropospheric inorganic aerosol burden could lead to an additional negative radiative forcing. Changes in these aerosols at the surface and the associated air quality implications are examined in Section 3.1.4.

~~In the stratosphere, total inorganic aerosol increases in the Cl_2 and Cl_2_BrCl_Br_2 scenarios due to increased sulfate (see Table S7). Stratospheric total inorganic aerosol in the hydrogen peroxide experiments decreases by ~2%. This does not impact stratospheric ozone.~~

3.1.4 Impacts on Surface Air Quality

Surface $PM_{2.5}$, CO, ozone, and NO_2 are air pollutants impacted by the atmospheric oxidation enhancement experiments. These largely follow the changes in tropospheric burdens (see Tables 2 and S6). Surface NO_2, however, was negligibly impacted by all experiments; most of the changes in tropospheric NO_x occurred in the upper troposphere (see Figure S5~~3~~). The change in global annual mean surface $PM_{2.5}$, CO, and ozone is shown in Figure ~~S4~~ S6 across the different scenarios, with spatial variations in annual mean surface $PM_{2.5}$ and ozone shown in Figures ~~3~~ 5 and ~~4~~6, respectively.

In the mean across all scenarios, there are declines in surface ozone ~~co-benefits~~air pollution (Figure S6~~4~~). Surface $PM_{2.5}$ increases in all scenarios except in the Chloride case, where in the absence of iron to mediate the Cl_2 release, the additional chloride leads to decreased sulfate and nitrate. Interestingly, H_2O_2_mid has worse air quality impacts than H_2O_2_high despite having less emissions; $PM_{2.5}$ increases more, and CO and ozone decrease less. There are larger impacts on $PM_{2.5}$ from the hydrogen peroxide and OH methods (up to 14–19 $\mu g/m^3$) than the Cl_2 and Cl_2_BrCl_Br_2 methods (up to 6–7 $\mu g/m^3$). These results are consistent with prior work suggesting that aerosol production can be oxidant-limited (e.g., Mayhew and Haskins, 2025; Shah et al., 2018). Figure ~~4~~2 shows the absolute change in $PM_{2.5}$ spatially in year 2019. Gray boxes highlight areas already in exceedance of the U.S. Environmental Protection Agency's (EPA's) annual mean $PM_{2.5}$ primary standard of 9 $\mu g\ m^{-3}$, which remain in exceedance when the experiment is applied. Black boxes highlight areas where the experiment to increase methane oxidation brought a region from <9 $\mu g\ m^{-3}$ to an exceedance of 9 $\mu g\ m^{-3}$. Blue boxes show where the experiment led to improved $PM_{2.5}$ from an exceedance to < 9 $\mu g\ m^{-3}$.

These results represent one single year of AOE application (2019). As such, the exact magnitude and spatial patterns of changes in annual mean $PM_{2.5}$ due to AOE may vary interannually due to variability in meteorology and its

effects on natural emissions, pollutant transport, and $PM_{2.5}$ removal, and the variability in background anthropogenic emissions. Moreover, long-term simulations using the CESM2 model suggest that relative changes in tropospheric sulfate aerosol and ozone due to Cl_2 gas-based AOE increase during the first 15 years of continuous application and then stabilize (Li, Meidan et al., 2023). Here, Figure 4 highlights the potential risks in surface $PM_{2.5}$ air quality in different regions in the initial years of deployment. Although the emissions for Cl_2 and Cl_2_BrCl_Br_2 are focused over the oceans, there are larger changes seen on land in both cases than over the oceans—with the exception of the Arctic ocean, where ammonium aerosol drives a larger increase (Figure ~~2~~4). The largest absolute increases in surface $PM_{2.5}$ in the ~~OH-based~~ hydrogen peroxide experiments ~~(not shown) are concentrated over northern hemisphere land including~~occur in Europe, India, China, ~~and~~ Russia, Equatorial Asia, and southern Africa~~. Hydrogen peroxide experiments follow a similar pattern but have reduced impact over North America and greater increases in South America and southern Africa~~ (Figure ~~2~~4). The impact of daytime-only emissions (not shown) varied depending on the level of hydrogen peroxide emissions; for the H_2O_2_mid scenario, daytime-only emissions had higher $PM_{2.5}$ concentrations, but for the H_2O_2_low scenario the daytime-only emissions reduced $PM_{2.5}$ concentrations. Similarly to the tropospheric-wide changes, these changes are driven by increases in sulfate with decreases in nitrate partially compensating, particularly in the Cl_2 and Cl_2_BrCl_Br_2 methods. ~~Surface organic aerosol also increases overall due to the increased atmospheric oxidation.~~ Decreases in nitrate lead to small decreases in total $PM_{2.5}$ in some regions in the Cl_2 scenario. Overall, AOE exacerbates existing $PM_{2.5}$ air quality issues in populated regions of Europe and Asia in year 2019 (Figure ~~2~~4).

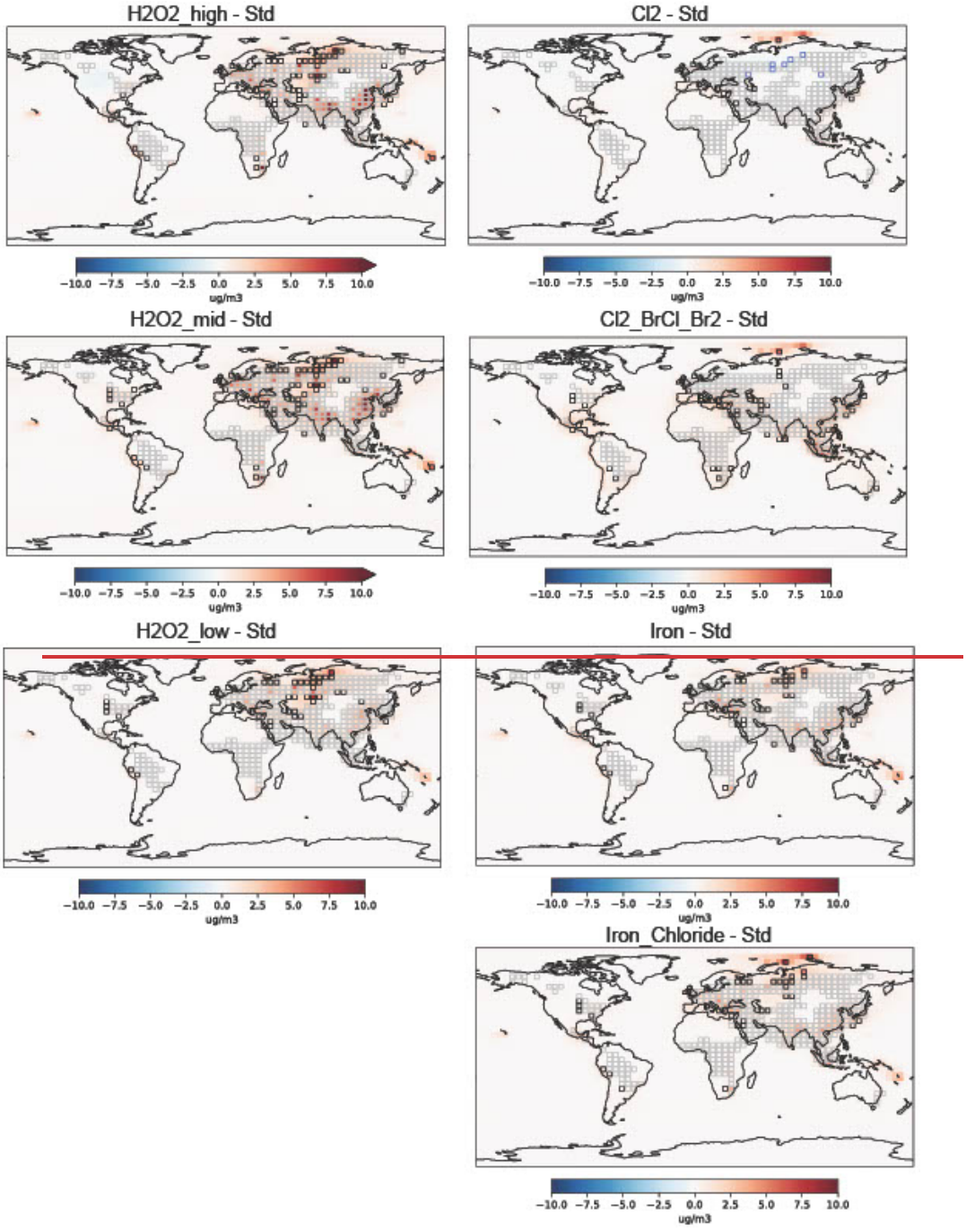
H2O2_high - Std
Cl2 - Std
H2O2_mid - Std
Cl2_BrCl_Br2 - Std
H2O2_low - Std
Iron - Std
Iron_Chloride - Std
−10.0 −7.5 −5.0 −2.5 0.0 2.5 5.0 7.5 10.0
ug/m3

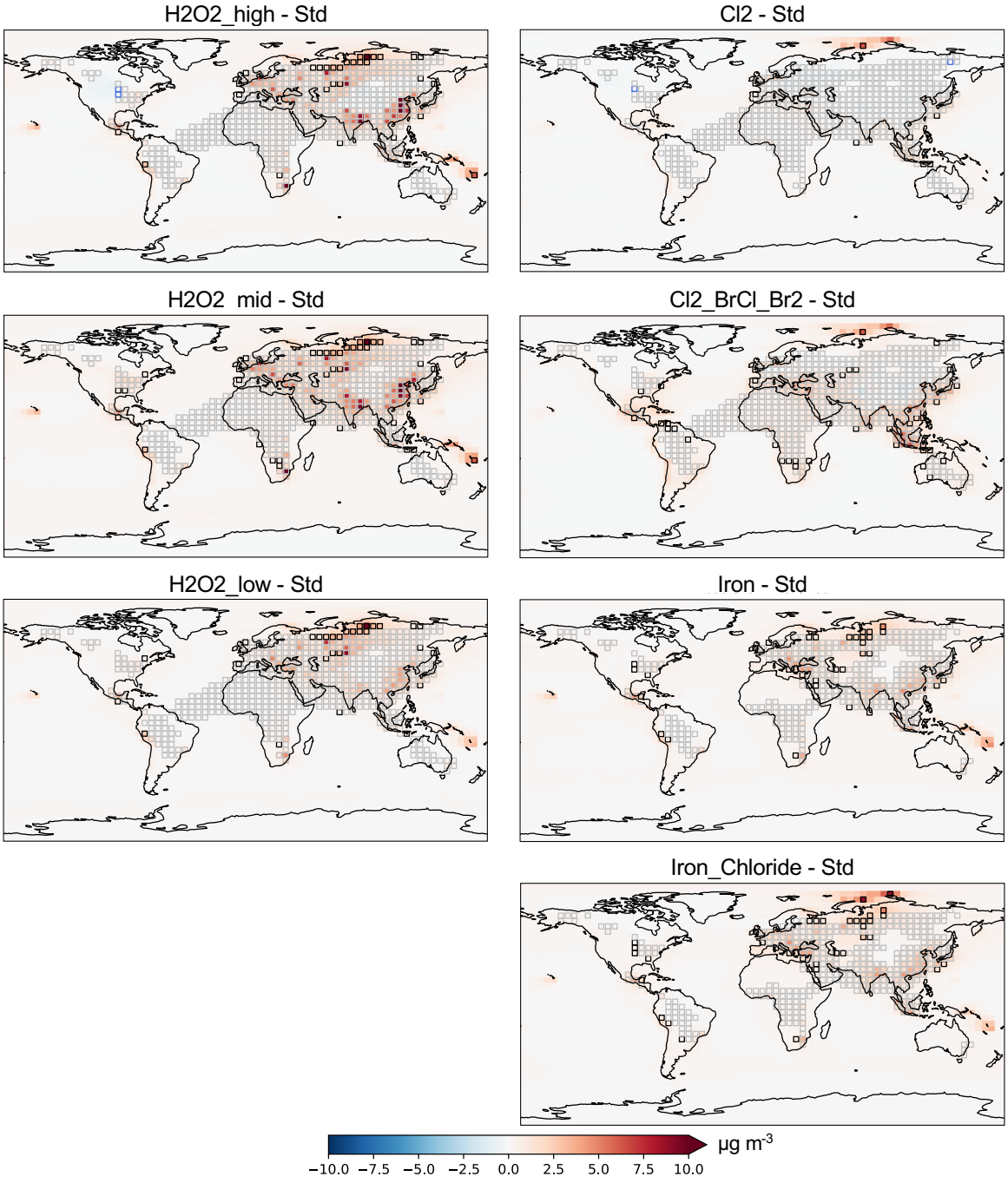

Figure ~~24~~: Absolute change in surface $PM_{2.5}$ relative to the standard model in year 2019. Gray boxes: areas already in exceedance of USEPA's annual mean $PM_{2.5}$ primary standard of 9 µg m^{-3}, which remain in exceedance when the experiment is applied. Black boxes: the experiment brought a region from <9 µg m^{-3} to an exceedance of ≥9 µg m^{-3}. Blue boxes: experiment led to improved $PM_{2.5}$ from an exceedance to < 9 µg m^{-3}.

Figure ~~3~~ 5 shows the absolute change in annual mean surface ozone across model experiments. In the global mean, surface ozone decreases on average in all methods (see Figure ~~S4~~S6), with largest mean decreases in the Cl_2_BrCl_Br_2 and H_2O_2_high experiments. At the same time, individual grid boxes in the hydrogen peroxide experiments see increases in annual mean ozone across populated areas (see Figure ~~3~~5). This has implications for the location of additional OH release, balancing the targeting of methane point sources versus populated areas where ozone may increase. Figure 3 again highlights that H_2O_2_mid has worse air quality impacts for ozone than H_2O_2_high.

Surface CO follows the tropospheric changes presented in Section 3.1.1 with decreases in hydrogen peroxide–based scenarios and increases in chlorine-based scenarios. Increases in surface CO concentrations in the chlorine-based scenarios are small relative to health guidelines and largely occur over the oceans. Surface CO decreases everywhere in the hydrogen peroxide–based experiments. These changes represent the short-term impact over 1 year of applied AOE.

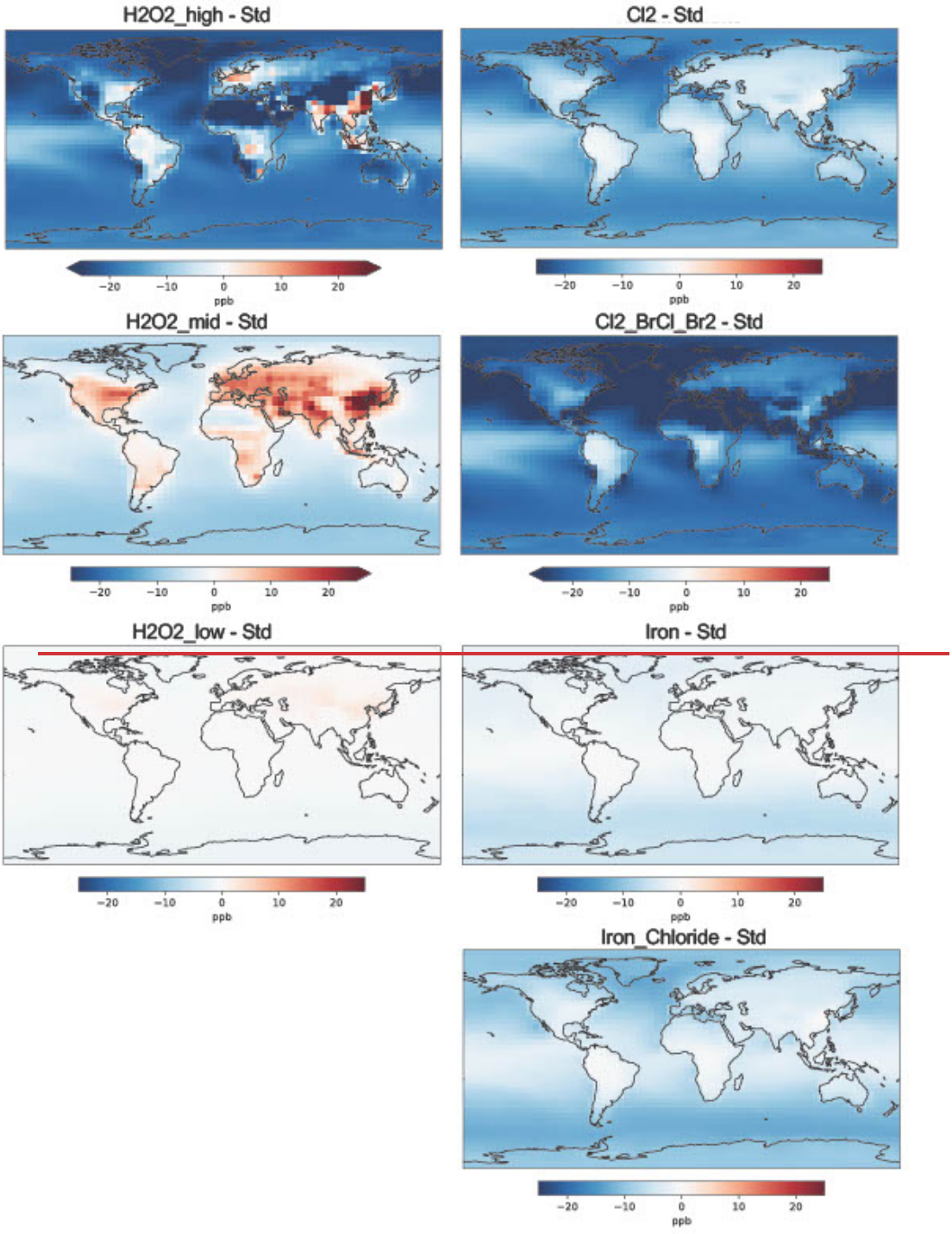
H2O2_high - Std
Cl2 - Std
H2O2_mid - Std
Cl2_BrCl_Br2 - Std
H2O2_low - Std
Iron - Std
Iron_Chloride - Std
−20
−10
0
10
20
ppb

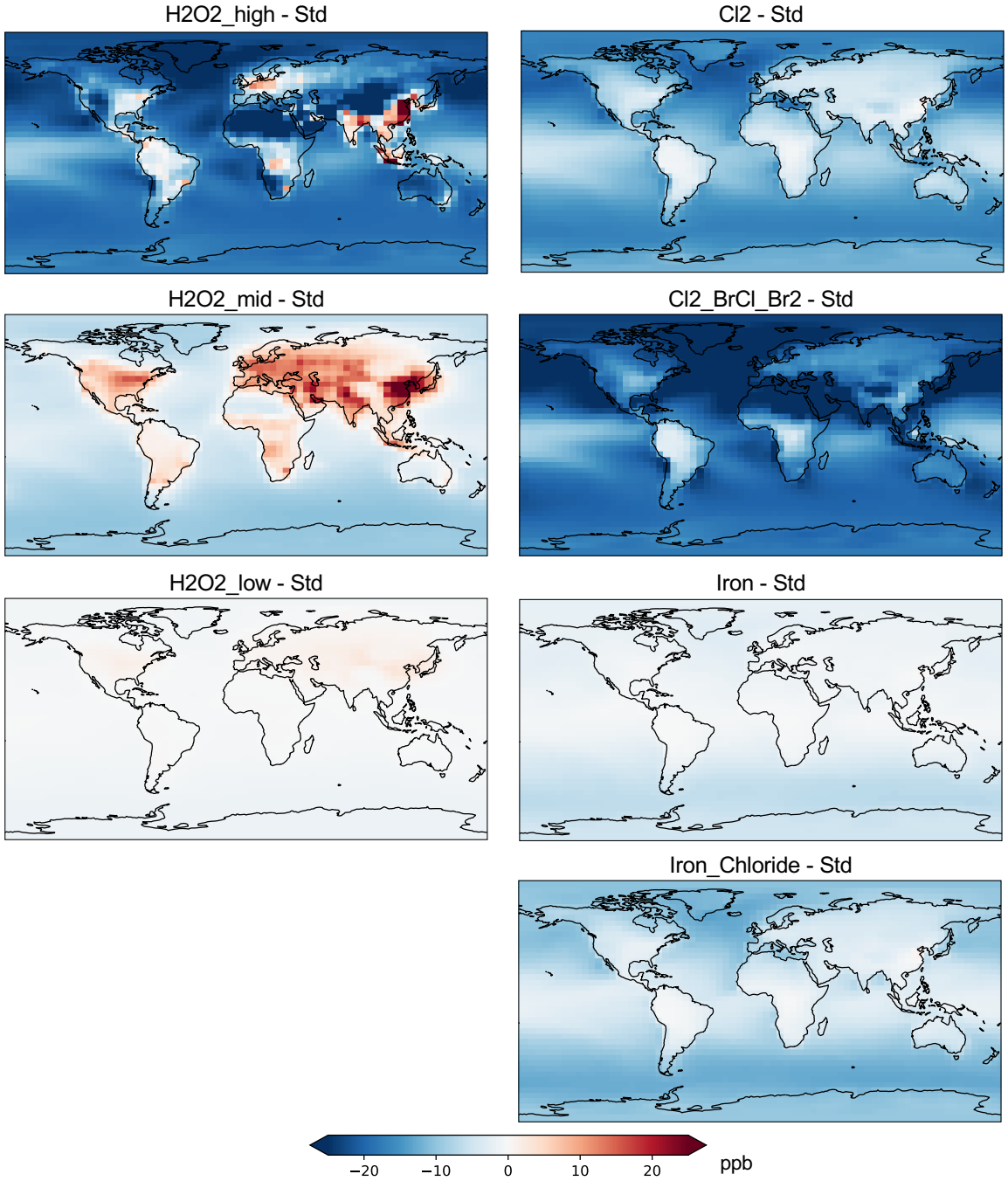

595 **Figure ~~3~~5: Absolute change in surface ozone (ppb) between model experiments detailed in Table 1 and the standard model in year 2019.**

3.1.5 Interactions with the Hydrogen Economy

Increases in hydrogen (H_2) emissions due to leakage from hydrogen applications will lead to a positive feedback on methane, as they react with OH and reduce the amount of OH available to oxidize methane (e.g., Bertagni et al., 2022; Ocko & Hamburg, 2022; Warwick et al., 2023). Based on results from a coupled Earth system model with interactive atmospheric chemistry, Warwick et al. (2023) find that increases in hydrogen alone lead to increases in methane, CO (whose main sink is also OH), and ozone. Hydrogen peroxide also increases (Warwick et al., 2023). A comparison with the results of the present study is shown in Table S8. A shift to hydrogen from fossil fuels, especially if the hydrogen is "green" (produced via renewable energy), will reduce emissions from fossil fuels including methane, CO, and NO_x. The net effect on methane thus depends on the amount of hydrogen produced and how it is produced (e.g., renewables or fossil fuels) as well as its leak rate (Bertagni et al., 2022; Ocko & Hamburg, 2022; Warwick et al., 2023).

How atmospheric oxidation enhancement may perform under a future global hydrogen economy also depends on how the hydrogen is produced and the leak rate. Based on the results of Warwick et al. (2023), a reasonable future global hydrogen economy scenario with a mid-range leak rate of 7% would lead to 1,000 ppb H_2 at the surface. Assuming 100% green hydrogen and thus concomitant reductions in fossil fuel emissions (including methane), OH concentrations decrease by 1% and the methane lifetime increases by 1.9% (Warwick et al., 2023). Without any reductions in fossil fuel emissions and a higher leak rate of 13% (1,500 ppb H_2 at the surface), OH concentrations decrease by 9.9% and the methane lifetime increases by 11.7% (Warwick et al., 2023). Reality will likely be somewhere in between. The effect of hydrogen emissions and emissions of hydrogen peroxide for atmospheric oxidation enhancement counteract each other (see Table S8). For chlorine, there is a synergistic effect on OH and CO.

At the same time, methane oxidation by OH eventually produces additional hydrogen (e.g., Bertagni et al., 2022). Based on Bertagni et al. (2022), the production of hydrogen from present methane oxidation from current OH could be approximately the same as future global hydrogen economy emissions with a 1% leak rate. In the current study, hydrogen is a species with globally fixed concentrations in GEOS-Chem, and thus this effect cannot be quantified. However, it is possible that the increased methane oxidation by OH in the hydrogen peroxide based scenarios could lead to increased atmospheric hydrogen, which would then react away some of the additional OH. Thus, more hydrogen peroxide would need to be emitted for the same effect on methane found in the current study if both the two-way feedback of methane oxidation on hydrogen and vice versa and future hydrogen emissions from a global energy transition are considered. For the Cl_2 experiment in the current study that leads to a decrease in methane, OH is significantly reduced (by 28%), which would decrease the source of hydrogen from methane oxidation by OH. The effects are likely nonlinear, and thus it is not clear whether chlorine mediated atmospheric oxidation enhancement would be less affected by the global hydrogen economy transition than OH-mediated atmospheric oxidation enhancement.

4 Uncertainties

Model resolution. Here I use a coarse-resolution global model simulation. This is not appropriate to examine point source applications near high methane emitters. Model resolution can lead to biases due to nonlinear atmospheric chemistry. However, these effects vary spatially and temporally and for tropospheric NO_2 in GEOS-Chem are within ±8% of high-resolution simulations (C. Li et al., 2023). Resolution effects are most important in polluted regions and are becoming less important as anthropogenic sources are reduced (C. Li et al., 2023). At the same time, Pennacchio et al. (2025) demonstrated the challenges in representing high-chlorine conditions in global lower-resolution models that result from point source emissions of iron for atmospheric methane oxidation enhancement, including how dilution of iron emission plumes and their interactions with the surrounding NO_x and ozone gradients can change the direction of the change in methane predicted.

Uncertainties in iron salt aerosol mechanism. Representation of chlorine release from iron salt aerosols in models remains highly parameterized. Complexities in iron solubility and speciation are not well represented. Depending on the reaction rate and representation, a given mass of iron salt aerosol release may lead to increases or decreases in the methane lifetime. Additional laboratory studies of natural and engineered iron salt aerosol, including mixtures with ambient species, are needed to improve the understanding of the kinetics and driving factors. Field studies and additional observations that could help evaluate this mechanism in models (e.g., isotopic composition, chloride, chlorine, iron and its speciation) will also aid in constraining this process.

Methods for OH release. The method and location of OH release will have different impacts. Here I only examined hydrogen peroxide as a mechanism for OH release, versus OH release without a specific mechanism. Effects of water vapor or artificial radiation for producing OH could have additional effects on climate forcers and air pollution.

Chemistry and time horizon. Here I use the "simple" SOA mechanism (fixed-yield, direct, and irreversible formation); additional simulations would be needed to better understand the change in SOA production under varying chemical regimes of OH and chlorine addition for methane oxidation. In addition, emissions are kept constant in year 2019. Most of the $PM_{2.5}$ effects predicted here are mediated by sulfate; future reductions in SO_2 emissions would likely limit this effect. We do not include interactive hydrogen (H_2) chemistry in our model simulation. Increased methane oxidation by OH in the hydrogen peroxide–based scenarios could lead to increased atmospheric H_2, as would potential future increases in hydrogen applications and their associated H_2 emissions from leakage. This would lead to a positive feedback on methane, as H_2 reacts with OH and reduces the amount of OH available to oxidize methane (e.g., Bertagni et al., 2022; Ocko & Hamburg, 2022; Warwick et al., 2023). As the simulations here are performed for only 1 year following 1 year of initialization, they cannot assess the stratospheric impact of AOE including on ozone depletion due to the long lifetime of air in the stratosphere. Over 30-year-long CESM2 simulations, Li, Meidan et al. (2023) find that chlorine-based AOE leads to stratospheric ozone depletion. Finally, uncertainties in the representation of halogen chemistry may impact the prediction of unintended consequences. For example, whether the halogen chemical mechanism includes interactions with sulfur seems to

lead to different results for how increased chlorine affects sulfate aerosol between this study (increases) and Li, Meidan et al. (2023) (decreases).

5 Conclusions

Here we simulate multiple scenarios of enhancing atmospheric methane oxidation via OH or Cl including hydrogen peroxide release, Cl_2 emissions, and iron salt aerosol in a global chemical transport model to assess the potential for decreasing the methane lifetime and resulting impacts on other climate forcers, stratospheric ozone, and surface air quality. The overall impacts of atmospheric oxidation enhancement methods on climate and human health involve multiple competing factors (see Figure 46).

Based on the present work, current global ~~demand~~ production of hydrogen peroxide is not sufficient to affect methane on a global scale, and this presents a challenge. Release of gas-phase Cl_2 is promising, but the exact mechanism to accomplish this and ensure it is large enough to reduce rather than increase methane remains a major challenge. Two different model approaches (this work, and Li, Meidan, et al., 2023) show that a large quantity of Cl_2 (>100–300 Tg/yr) must be added to the atmosphere in order to have an impact. Smaller amounts, or increasing particulate chloride as shown in this study, will increase methane. Here we find that emitting particulate iron alone to catalyze chlorine release from sea salt aerosol following the reaction rate parameterization from Chen et al. (2024) ~~does not~~can release sufficient Cl_2 to decrease global methane by 2.5% but requires larger emissions than in previous studies (565 Tg/yr) to accomplish a smaller change.

In addition to the impacts on methane, increased atmospheric oxidation via hydrogen peroxide- and chlorine-based methods largely has a climate co-benefit, via increased tropospheric aerosols and decreased tropospheric ozone. Chlorine-based methods increase other greenhouse gases and thus have reduced climate co-benefits.

Overall, ozone-depleting substances are increased in chlorine-based methods and decreased in OH-based methods. Most of the species impacted are short-lived. ~~Here I predict minimal reductions in stratospheric ozone, with the exception of the chlorine experiment that includes bromine contamination.~~ Longer simulations are needed to understand the full impacts on stratospheric chemistry.

Chlorine-based methods reduce surface ozone air pollution. OH-based methods largely result in ozone reductions as well but lead to increases in ozone in already polluted areas. Surface $PM_{2.5}$ pollution increases over land and in highly populated regions across most chlorine scenarios and all OH-based methods, regardless of whether emissions are limited to the oceans. These increases are on the order of present EPA air quality standards for annual mean $PM_{2.5}$. These results from a one-year simulation highlight potential risks to air quality during the initial phases of AOE deployment.

Co-emission of bromine with chlorine appears to remove any benefit from chlorine-based approaches. In the case of 20% bromine release by mass with respect to chlorine, the methane lifetime ~~nearly doubles~~increases by 6.7%. The addition of bromine also generally results in worse outcomes with respect to surface air quality, halogenated greenhouse gases, and

~~stratospheric ozone~~ozone-depleting substances. Additional experimental measurements of bromine species released from natural and engineered iron salt aerosol are needed to constrain these effects.

Overall, additional research in higher-resolution, longer-term modeling frameworks as well as laboratory experiments is needed to constrain whether the AOE methods have the desired intended consequences of sufficiently decreasing atmospheric methane, and the risk level for the unintended consequences of potential increases in halogenated greenhouse gases, ozone-depleting substances, and particulate matter air pollution.

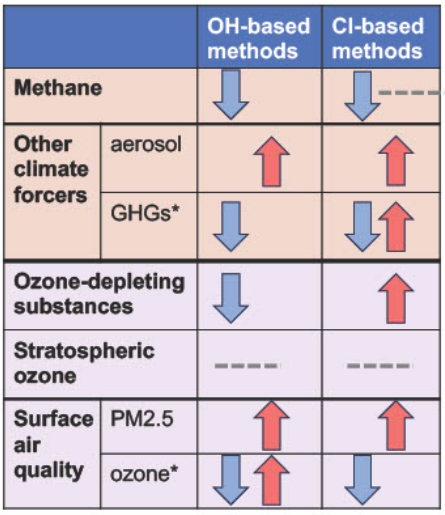

Figure 64: The overall impacts of atmospheric oxidation enhancement methods on climate and human health involve multiple competing factors. Note: * = sign of change depends on species (greenhouse gases [GHGs]) or location (ozone).

Competing interests. The contact author has declared that there are no competing interests.

Acknowledgments. I acknowledge helpful discussions with Jessica Haskins, Katherine Travis, and Qianjie Chen, and funding from the National Academyies of Sciences contract PO-10000845. Portions are reproduced with permission from the National Academy of Sciences, Courtesy of the National Academies Press, Washington, D.C.

Data Availability. The model data used in this study will be made available with a permanent DOI when the review process is complete through the Illinois Data Bank (https://databank.illinois.edu/) and will be subject to the terms of the Creative Commons Attribution 4.0 International (CC BY 4.0). The standard model code is available at https://doi.org/10.5281/zenodo.5500717. For the review process, model data is temporarily available at the following link: https://www.dropbox.com/scl/fo/rtktddj7cru74p200x5q5/AI91DLtDyZJaXJlJEPY4j8Y?rlkey=x0yt2wjkxb9agv3gf4hwvh57q&st=0l0vx6az&dl=0

References

Abernethy, S., Kessler, M. I., & Jackson, R. B. (2023). Assessing the potential benefits of methane oxidation technologies using a concentration-based framework. *Environmental Research Letters*, *18*(9), Article 094064. https://doi.org/10.1088/1748-9326/acf603

Alexander, B., Park, R. J., Jacob, D. J., & Gong, S. (2009). Transition metal-catalyzed oxidation of atmospheric sulfur: Global implications for the sulfur budget. *Journal of Geophysical Research*, *114*(D2). https://doi.org/10.1029/2008JD010486

Allan, W., Struthers, H., & Lowe, D. C. (2007). Methane carbon isotope effects caused by atomic chlorine in the marine boundary layer: Global model results compared with Southern Hemisphere measurements. *Journal of Geophysical Research: Atmospheres*, *112*(D4). https://doi.org/10.1029/2006JD007369

Amos, H. M., Jacob, D. J., Holmes, C. D., Fisher, J. A., Wang, Q., Yantosca, R. M., Corbitt, E. S., Galarneau, E., Rutter, A. P., Gustin, M. S., Steffen, A., Schauer, J. J., Graydon, J. A., St. Louis, V. L., Talbot, R. W., Edgerton, E. S., Zhang, Y., & Sunderland, E. M. (2012). Gas-particle partitioning of atmospheric Hg(II) and its effect on global mercury deposition. *Atmospheric Chemistry and Physics*, *12*(1), 591–603. https://doi.org/10.5194/acp-12-591-2012

Bell, S. C. (2023). WO2023108278 - Systems and Methods for Atmospheric Dispersion of Oxidant for Net Conversion of Atmospheric Methane to Carbon Dioxide.

Bertagni, M. B., Pacala, S. W., Paulot, F., & Porporato, A. (2022). Risk of the hydrogen economy for atmospheric methane. *Nature Communications*, *13*, Article 7706. https://doi.org/10.1038/s41467-022-35419-7

Chen, Q., Schmidt, J. A., Shah, V., Jaeglé, L., Sherwen, T., & Alexander, B. (2017). Sulfate production by reactive bromine: Implications for the global sulfur and reactive bromine budgets. *Geophysical Research Letters*, *44*(13), 7069–7078. https://doi.org/10.1002/2017GL073812

Chen, Q., Wang, X., Fu, X., Li, X., Alexander, B., Peng, X., Wang, W., Xia, M., Tan, Y., Gao, J., Chen, J., Mu, Y., Liu, P., & Wang, T. (2024). Impact of molecular chlorine production from aerosol iron photochemistry on atmospheric oxidative capacity in North China. *Environmental Science & Technology, 58*(28), 12585–12597. https://doi.org/10.1021/acs.est.4c02534

Eastham, S. D., Fritz, T., Sanz-Morère, I., Prashanth, P., Allroggen, F., Prinn, R. G., Speth, R. L., & Barrett, S. R. H. (2022). Impacts of a near-future supersonic aircraft fleet on atmospheric composition and climate. *Environmental Science: Atmospheres*, *2*(3), 388–403. https://doi.org/10.1039/D1EA00081K

Eastham, S. D., Weisenstein, D. K., & Barrett, S. R. H. (2014). Development and evaluation of the unified tropospheric–stratospheric chemistry extension (UCX) for the global chemistry-transport model GEOS-Chem. *Atmospheric Environment*, *89*, 52–63. https://doi.org/10.1016/j.atmosenv.2014.02.001

Fairlie, T. D., Jacob, D. J., & Park, R. J. (2007). The impact of transpacific transport of mineral dust in the United States. *Atmospheric Environment*, *41*(6), 1251–1266. https://doi.org/10.1016/j.atmosenv.2006.09.048

Fisher, J. A., Atlas, E. L., Barletta, B., Meinardi, S., Blake, D. R., Thompson, C. R., Ryerson, T. B., Peischl, J., Tzompa-Sosa, Z. A., & Murray, L. T. (2018). Methyl, ethyl, and propyl nitrates: Global distribution and impacts on reactive nitrogen in remote marine environments. *Journal of Geophysical Research: Atmospheres*, *123*(21), 12429–12451. https://doi.org/10.1029/2018JD029046

Fisher, J. A., Jacob, D. J., Travis, K. R., Kim, P. S., Marais, E. A., Chan Miller, C., Yu, K., Zhu, L., Yantosca, R. M., Sulprizio, M. P., Mao, J., Wennberg, P. O., Crounse, J. D., Teng, A. P., Nguyen, T. B., St. Clair, J. M., Cohen, R. C., Romer, P., Nault, B. A., … Mikoviny, T. (2016). Organic nitrate chemistry and its implications for nitrogen budgets in an isoprene- and monoterpene-rich atmosphere: Constraints from aircraft (SEAC^{4}RS) and ground-based (SOAS) observations in the Southeast US. *Atmospheric Chemistry and Physics*, *16*(9), 5969–5991. https://doi.org/10.5194/acp-16-5969-2016

Gelaro, R., McCarty, W., Suárez, M. J., Todling, R., Molod, A., Takacs, L., Randles, C. A., Darmenov, A., Bosilovich, M. G., Reichle, R., Wargan, K., Coy, L., Cullather, R., Draper, C., Akella, S., Buchard, V., Conaty, A., Da Silva, A. M., Gu, W., … Zhao, B. (2017). The Modern-Era Retrospective Analysis for Research and Applications, version 2 (MERRA-2). *Journal of Climate*, *30*(14), 5419–5454. https://doi.org/10.1175/JCLI-D-16-0758.1

Gorham, K. A., Abernethy, S., Jones, T. R., Hess, P., Mahowald, N. M., Meidan, D., Johnson, M. S., van Herpen, M. M. J. W., Xu, Y., Saiz-Lopez, A., Röckmann, T., Brashear, C. A., Reinhardt, E., and Mann, D.: Opinion: A research roadmap for exploring atmospheric methane removal via iron salt aerosol, Atmos. Chem. Phys., 24, 5659–5670, https://doi.org/10.5194/acp-24-5659-2024, 2024. ~~Gorham, K., Abernethy, S., Jones, T. R., Hess, P., Mahowald, N. M., Meidan, D., Johnson, M. S., van Herpen, M. M. J. W., Xu, Y., Saiz-Lopez, A., Röckmann, T., Brashear, C., Reinhardt, E., & Mann, D. (2023). *Exploring potential atmospheric methane removal approaches: An example research roadmap for chlorine radical enhancement* [Preprint]. ESS Open Archive. https://doi.org/10.22541/essoar.169755495.51174285/v1~~

Gromov, S., Brenninkmeijer, C. A. M., & Jöckel, P. (2018). A very limited role of tropospheric chlorine as a sink of the greenhouse gas methane. *Atmospheric Chemistry and Physics*, *18*(13), 9831–9843. https://doi.org/10.5194/acp-18-9831-2018

Guenther, A. B., Jiang, X., Heald, C. L., Sakulyanontvittaya, T., Duhl, T., Emmons, L. K., & Wang, X. (2012). The Model of Emissions of Gases and Aerosols from Nature version 2.1 (MEGAN2.1): An extended and updated framework for modeling biogenic emissions. *Geoscientific Model Development*, *5*(6), 1471–1492. https://doi.org/10.5194/gmd-5-1471-2012

Holmes, C. D. (2018). Methane feedback on atmospheric chemistry: Methods, models, and mechanisms. *Journal of Advances in Modeling Earth Systems*, *10*(4), 1087–1099. https://doi.org/10.1002/2017MS001196

Holmes, C. D., Bertram, T. H., Confer, K. L., Graham, K. A., Ronan, A. C., Wirks, C. K., & Shah, V. (2019). The role of clouds in the tropospheric NO_x cycle: A new modeling approach for cloud chemistry and its global implications. *Geophysical Research Letters*, *46*(9), 4980–4990. https://doi.org/10.1029/2019GL081990

Holmes, C. D., Prather, M. J., Søvde, O. A., & Myhre, G. (2013). Future methane, hydroxyl, and their uncertainties: Key climate and emission parameters for future predictions. *Atmospheric Chemistry and Physics*, *13*(1), 285–302. https://doi.org/10.5194/acp-13-285-2013

Horowitz, H. M., Holmes, C., Wright, A., Sherwen, T., Wang, X., Evans, M., Huang, J., Jaeglé, L., Chen, Q., Zhai, S., & Alexander, B. (2020). Effects of sea salt aerosol emissions for marine cloud brightening on atmospheric chemistry: Implications for radiative forcing. *Geophysical Research Letters*, *47*(4), Article e2019GL085838. https://doi.org/10.1029/2019GL085838

Hossaini, R., Chipperfield, M. P., Montzka, S. A., Leeson, A. A., Dhomse, S. S., & Pyle, J. A. (2017). The increasing threat to stratospheric ozone from dichloromethane. *Nature Communications*, *8*(1), Article 15962. https://doi.org/10.1038/ncomms15962

Hossaini, R., Chipperfield, M. P., Saiz-Lopez, A., Fernandez, R., Monks, S., Feng, W., Brauer, P., & Von Glasow, R. (2016). A global model of tropospheric chlorine chemistry: Organic versus inorganic sources and impact on methane oxidation. *Journal of Geophysical Research: Atmospheres*, *121*(23), 14271–14297. https://doi.org/10.1002/2016JD025756

Huang, J., & Jaeglé, L. (2017). Wintertime enhancements of sea salt aerosol in polar regions consistent with a sea ice source from blowing snow. *Atmospheric Chemistry and Physics*, *17*(5), 3699–3712. https://doi.org/10.5194/acp-17-3699-2017

Jaeglé, L., Quinn, P. K., Bates, T. S., Alexander, B., & Lin, J.-T. (2011). Global distribution of sea salt aerosols: New constraints from in situ and remote sensing observations. *Atmospheric Chemistry and Physics*, *11*(7), 3137–3157. https://doi.org/10.5194/acp-11-3137-2011

Johnson, M. S., E. J. K. Nilsson, E. A. Svensson, S. Langer, Gas Phase Advanced Oxidation for Effective, Efficient In Situ Control of Pollution, Environmental Science & Technology 48(15), 8768–8776, 2014.

Khodayari, A., Olsen, S. C., Wuebbles, D. J., & Phoenix, D. B. (2015). Aviation NO_x-induced CH_4 effect: Fixed mixing ratio boundary conditions versus flux boundary conditions. *Atmospheric Environment*, *113*, 135–139. https://doi.org/10.1016/j.atmosenv.2015.04.070

Li, C., Martin, R. V., Cohen, R. C., Bindle, L., Zhang, D., Chatterjee, D., Weng, H., & Lin, J. (2023). Variable effects of spatial resolution on modeling of nitrogen oxides. *Atmospheric Chemistry and Physics*, *23*(5), 3031–3049. https://doi.org/10.5194/acp-23-3031-2023

Li, Q., Fernandez, R. P., Hossaini, R., Iglesias-Suarez, F., Cuevas, C. A., Apel, E. C., Kinnison, D. E., Lamarque, J.-F., & Saiz-Lopez, A. (2022). Reactive halogens increase the global methane lifetime and radiative forcing in the 21st century. *Nature Communications*, *13*(1), Article 2768. https://doi.org/10.1038/s41467-022-30456-8

Li, Q., Meidan, D., Hess, P., Añel, J. A., Cuevas, C. A., Doney, S., Fernandez, R. P., Van Herpen, M., Höglund-Isaksson, L., Johnson, M. S., Kinnison, D. E., Lamarque, J.-F., Röckmann, T., Mahowald, N. M., & Saiz-Lopez, A. (2023). Global environmental implications of atmospheric methane removal through chlorine-mediated chemistry-climate interactions. *Nature Communications*, *14*(1), Article 4045. https://doi.org/10.1038/s41467-023-39794-7

Lin, H., Jacob, D. J., Lundgren, E. W., Sulprizio, M. P., Keller, C. A., Fritz, T. M., Eastham, S. D., Emmons, L. K., Campbell, P. C., Baker, B., Saylor, R. D., & Montuoro, R. (2021). Harmonized Emissions Component (HEMCO) 3.0 as a versatile emissions component for atmospheric models: Application in the GEOS-Chem, NASA GEOS, WRF-GC,

CESM2, NOAA GEFS-Aerosol, and NOAA UFS models. *Geoscientific Model Development*, *14*(9), 5487–5506. https://doi.org/10.5194/gmd-14-5487-2021

Lin, J.-T., and M. McElroy, *Impacts of boundary layer mixing on pollutant vertical profiles in the lower troposphere: Implications to satellite remote sensing*, Atmospheric Environment, **44**(14), 1726-1739, doi:10.1016/j.atmosenv.2010.02.009, 2010.

Liu, H., Jacob, D. J., Bey, I., & Yantosca, R. M. (2001). Constraints from ^{210}Pb and ^{7}Be on wet deposition and transport in a global three-dimensional chemical tracer model driven by assimilated meteorological fields. *Journal of Geophysical Research: Atmospheres*, *106*(D11), 12109–12128. https://doi.org/10.1029/2000JD900839

Mao, J., Jacob, D. J., Evans, M. J., Olson, J. R., Ren, X., Brune, W. H., Clair, J. M. St., Crounse, J. D., Spencer, K. M., Beaver, M. R., Wennberg, P. O., Cubison, M. J., Jimenez, J. L., Fried, A., Weibring, P., Walega, J. G., Hall, S. R., Weinheimer, A. J., Cohen, R. C., Chen, G., Crawford, J. H., McNaughton, C., Clarke, A. D., Jaeglé, L., Fisher, J. A., Yantosca, R. M., Le Sager, P., and Carouge, C.: Chemistry of hydrogen oxide radicals (HO_x) in the Arctic troposphere in spring, Atmos. Chem. Phys., 10, 5823–5838, https://doi.org/10.5194/acp-10-5823-2010, 2010.

Mayhew, A. W., & Haskins, J. D. (2025). Potential air quality side-effects of emitting H2O2 to enhance methane oxidation as a climate solution. Environmental Science & Technology, 59(1), 679–688.

McDuffie, E. E., Fibiger, D. L., Dubé, W. P., Lopez-Hilfiker, F., Lee, B. H., Thornton, J. A., Shah, V., Jaeglé, L., Guo, H., Weber, R. J., Reeves, J. M., Weinheimer, A. J., Schroder, J. C., Campuzano-Jost, P., Jimenez, J. L., Dibb, J. E., Veres, P., Ebben, C., Sparks, T. L., … Brown, S. S. (2018). Heterogeneous N_2O_5 uptake during winter: Aircraft measurements during the 2015 WINTER campaign and critical evaluation of current parameterizations. *Journal of Geophysical Research: Atmospheres*, *123*(8), 4345–4372. https://doi.org/10.1002/2018JD028336

Meidan, D., Li, Q., Cuevas, C. A., Doney, S. C., Fernandez, R. P., Van Herpen, M. M. J. W., Johnson, M. S., Kinnison, D. E., Li, L., Hamilton, D. S., Saiz-Lopez, A., Hess, P., & Mahowald, N. M. (2024). Evaluating the potential of iron-based interventions in methane reduction and climate mitigation. *Environmental Research Letters*, *19*(5), Article 054023. https://doi.org/10.1088/1748-9326/ad3d72

Moffet, R. C.; Furutani, H.; Rödel, T. C.; Henn, T. R.; Sprau, P. O.; Laskin, A.; Uematsu, M.; Gilles, M. K. Iron Speciation and Mixing in Single Aerosol Particles from the Asian Continental Outflow. *J. Geophys. Res.* 2012, *117*, No. D07204.

Ming, T., Li, W., Yuan, Q., Davies, P., de Richter, R., Peng, C., Deng, Q., Yuan, Y., Caillol, S., & Zhou, N. (2022). Perspectives on removal of atmospheric methane. *Advances in Applied Energy*, *5*, Article 100085. https://doi.org/10.1016/j.adapen.2022.100085

Moffet, R. C., Furutani, H., Rödel, T. C., Henn, T. R., Sprau, P. O., Laskin, A., Uematsu, M., & Gilles, M. K. (2012). Iron speciation and mixing in single aerosol particles from the Asian continental outflow: Aerosol iron speciation in Asian outflow. *Journal of Geophysical Research: Atmospheres*, *117*(D7). https://doi.org/10.1029/2011JD016746

Murray, L. T. (2016). Lightning NO_x and impacts on air quality. *Current Pollution Reports*, *2*(2), 115–133. https://doi.org/10.1007/s40726-016-0031-7

Murray, L. T., Fiore, A. M., Shindell, D. T., Naik, V., & Horowitz, L. W. (2021). Large uncertainties in global hydroxyl projections tied to fate of reactive nitrogen and carbon. *Proceedings of the National Academy of Sciences*, *118*(43), Article e2115204118. https://doi.org/10.1073/pnas.2115204118

National Academies of Sciences, Engineering and Medicine (NASEM) report [2024] 'A Research Agenda Toward Atmospheric Methane Removal'

Neu, J., Prather, M., and Penner, J.: Global atmospheric chemistry: integrating over fractional cloud cover, J. Geophys. Res., 112, D11306, 12 pp., doi:10.1029/2006JD008007, 2007.

Ocko, I. B., & Hamburg, S. P. (2022). Climate consequences of hydrogen emissions. *Atmospheric Chemistry and Physics*, *22*(14), 9349–9368. https://doi.org/10.5194/acp-22-9349-2022

O'Connor, F. M., Johnson, B. T., Jamil, O., Andrews, T., Mulcahy, J. P., & Manners, J. (2022). Apportionment of the pre-industrial to present-day climate forcing by methane using UKESM1: The role of the cloud radiative effect. *Journal of Advances in Modeling Earth Systems*, *14*(10), Article e2022MS002991. https://doi.org/10.1029/2022MS002991

Oeste, F. D., de Richter, R., Ming, T., & Caillol, S. (2017). Climate engineering by mimicking natural dust climate control: The iron salt aerosol method. *Earth System Dynamics*, *8*(1), 1–54. https://doi.org/10.5194/esd-8-1-2017

Ordóñez, C., Lamarque, J.-F., Tilmes, S., Kinnison, D. E., Atlas, E. L., Blake, D. R., Sousa Santos, G., Brasseur, G., & Saiz-Lopez, A. (2012). Bromine and iodine chemistry in a global chemistry-climate model: Description and evaluation of very short-lived oceanic sources. *Atmospheric Chemistry and Physics*, *12*(3), 1423–1447. https://doi.org/10.5194/acp-12-1423-2012

Pai, S. J., Heald, C. L., Pierce, J. R., Farina, S. C., Marais, E. A., Jimenez, J. L., Campuzano-Jost, P., Nault, B. A., Middlebrook, A. M., Coe, H., Shilling, J. E., Bahreini, R., Dingle, J. H., & Vu, K. (2020). An evaluation of global organic aerosol schemes using airborne observations. *Atmospheric Chemistry and Physics*, *20*(5), 2637–2665. https://doi.org/10.5194/acp-20-2637-2020

Pennacchio, L., Mikkelsen, M. K., Krogsbøll, M., van Herpen, M., and Johnson, M. S. (2024). Physical and practical constraints on atmospheric methane removal technologies. Environmental Research Letters, 19(10), 104058.

Pennacchio, L.; van Herpen, M.; Meidan, D.; Saiz-Lopez, A.; Johnson, M. S. Catalytic Efficiencies for Methane Removal: Impact of HO x, NO x, and Chemistry in the High-Chlorine Regime. *ACS Earth Space Chem.* **2025**, *9*, 504– 512, DOI: 10.1021/acsearthspacechem.4c00283

Philip, S., Martin, R. V., Snider, G., Weagle, C. L., Van Donkelaar, A., Brauer, M., Henze, D. K., Klimont, Z., Venkataraman, C., Guttikunda, S. K., & Zhang, Q. (2017). Anthropogenic fugitive, combustion and industrial dust is a significant, underrepresented fine particulate matter source in global atmospheric models. *Environmental Research Letters*, *12*(4), Article 044018. https://doi.org/10.1088/1748-9326/aa65a4

Platt, U., Allan, W., & Lowe, D. (2004). Hemispheric average Cl atom concentration from $^{13}C/^{12}C$ ratios in atmospheric methane. *Atmospheric Chemistry and Physics*, *4*(9/10), 2393–2399. https://doi.org/10.5194/acp-4-2393-2004

Pound, R. J., Sherwen, T., Helmig, D., Carpenter, L. J., & Evans, M. J. (2020). Influences of oceanic ozone deposition on tropospheric photochemistry. *Atmospheric Chemistry and Physics*, *20*(7), 4227–4239. https://doi.org/10.5194/acp-20-4227-2020

Research and Markets. (2023). *Global hydrogen peroxide market analysis: Plant capacity, production, operating efficiency, technology, demand & supply, end user industries, distribution channel, regional demand, 2015-2030*. https://www.researchandmarkets.com/reports/5174562/global-hydrogen-peroxide-market-analysis-plant

Saiz-Lopez, A., Fernandez, R. P., Ordóñez, C., Kinnison, D. E., Gómez Martín, J. C., Lamarque, J.-F., & Tilmes, S. (2014). Iodine chemistry in the troposphere and its effect on ozone. *Atmospheric Chemistry and Physics*, *14*(23), 13119–13143. https://doi.org/10.5194/acp-14-13119-2014

V. Shah, L. Jaeglé, J.A. Thornton, F.D. Lopez-Hilfiker, B.H. Lee, J.C. Schroder, P. Campuzano-Jost, J.L. Jimenez, H. Guo, A.P. Sullivan, R.J. Weber, J.R. Green, M.N. Fiddler, S. Bililign, T.L. Campos, M. Stell, A.J. Weinheimer, D.D. Montzka, & S.S. Brown, Chemical feedbacks weaken the wintertime response of particulate sulfate and nitrate to emissions reductions over the eastern United States, Proc. Natl. Acad. Sci. U.S.A. 115 (32) 8110-8115, https://doi.org/10.1073/pnas.1803295115 (2018).

Shao, J., Chen, Q., Wang, Y., Lu, X., He, P., Sun, Y., Shah, V., Martin, R. V., Philip, S., Song, S., Zhao, Y., Xie, Z., Zhang, L., & Alexander, B. (2019). Heterogeneous sulfate aerosol formation mechanisms during wintertime Chinese haze events: Air quality model assessment using observations of sulfate oxygen isotopes in Beijing. *Atmospheric Chemistry and Physics*, *19*(9), 6107–6123. https://doi.org/10.5194/acp-19-6107-2019

Sherwen, T., Evans, M. J., Carpenter, L. J., Andrews, S. J., Lidster, R. T., Dix, B., Koenig, T. K., Sinreich, R., Ortega, I., Volkamer, R., Saiz-Lopez, A., Prados-Roman, C., Mahajan, A. S., & Ordóñez, C. (2016a). Iodine's impact on tropospheric oxidants: A global model study in GEOS-Chem. *Atmospheric Chemistry and Physics*, *16*(2), 1161–1186. https://doi.org/10.5194/acp-16-1161-2016

Sherwen, T., Schmidt, J. A., Evans, M. J., Carpenter, L. J., Großmann, K., Eastham, S. D., Jacob, D. J., Dix, B., Koenig, T. K., Sinreich, R., Ortega, I., Volkamer, R., Saiz-Lopez, A., Prados-Roman, C., Mahajan, A. S., & Ordóñez, C. (2016b). Global impacts of tropospheric halogens (Cl, Br, I) on oxidants and composition in GEOS-Chem. *Atmospheric Chemistry and Physics*, *16*(18), 12239–12271. https://doi.org/10.5194/acp-16-12239-2016

Shi, J., Guan, Y., Gao, H., Yao, X., Wang, R., & Zhang, D. (2022). Aerosol iron solubility specification in the global marine atmosphere with machine learning. *Environmental Science & Technology*, *56*(22), 16453–16461. https://doi.org/10.1021/acs.est.2c05266

Smith, C., Nicholls, Z. R. J., Armour, K., Collins, W., Forster, P., Meinshausen, M., Palmer, M. D., & Watanabe, M. (2021). The Earth's energy budget, climate feedbacks and climate sensitivity supplementary material. In V. Masson-Delmotte, P. Zhai, A. Pirani, S. L. Connors, C. Péan, S. Berger, N. Caud, Y. Chen, L. Goldfarb, M. I. Gomis, M. Huang, K. Leitzell, E. Lonnoy, J. B. R. Matthews, T. K. Maycock, T. Waterfield, Ö. Yelekçi, R. Yu, & B. Zhou (Eds.), *Climate change 2021: The physical science basis. Contribution of working group I to the Sixth Assessment Report of the*

Intergovernmental Panel on Climate Change. https://www.ipcc.ch/report/ar6/wg1/downloads/report/IPCC_AR6_WGI_Chapter07_SM.pdf

Tao, T., Wang, Y., Ming, T., Mu, L., de Richter, R., & Li, W. (2023). Downdraft energy tower for negative emissions: Analysis on methane removal and other co-benefits. *Greenhouse Gases: Science and Technology*, *13*(5), 713–720. https://doi.org/10.1002/ghg.2233

Taylor, S. R., & McLennan, S. M. (1985). *The continental crust: Its composition and evolution*. https://www.osti.gov/biblio/6582885

Trapp, J. M., Millero, F. J., & Prospero, J. M. (2010). Trends in the solubility of iron in dust-dominated aerosols in the equatorial Atlantic trade winds: Importance of iron speciation and sources: Fe solubility in North Atlantic trade wind aerosols. *Geochemistry, Geophysics, Geosystems*, *11*(3). https://doi.org/10.1029/2009GC002651

van Herpen, M. M. J. W., Li, Q., Saiz-Lopez, A., Liisberg, J. B., Röckmann, T., Cuevas, C. A., Fernandez, R. P., Mak, J. E., Mahowald, N. M., Hess, P., Meidan, D., Stuut, J.-B. W., & Johnson, M. S. (2023). Photocatalytic chlorine atom production on mineral dust–sea spray aerosols over the North Atlantic. *Proceedings of the National Academy of Sciences*, *120*(31), Article e2303974120. https://doi.org/10.1073/pnas.2303974120

Wang, Q., Jacob, D. J., Spackman, J. R., Perring, A. E., Schwarz, J. P., Moteki, N., Marais, E. A., Ge, C., Wang, J., & Barrett, S. R. H. (2014). Global budget and radiative forcing of black carbon aerosol: Constraints from pole-to-pole (HIPPO) observations across the Pacific. *Journal of Geophysical Research: Atmospheres*, *119*(1), 195–206. https://doi.org/10.1002/2013JD020824

Wang, X., Jacob, D. J., Downs, W., Zhai, S., Zhu, L., Shah, V., Holmes, C. D., Sherwen, T., Alexander, B., Evans, M. J., Eastham, S. D., Neuman, J. A., Veres, P. R., Koenig, T. K., Volkamer, R., Huey, L. G., Bannan, T. J., Percival, C. J., Lee, B. H., & Thornton, J. A. (2021). Global tropospheric halogen (Cl, Br, I) chemistry and its impact on oxidants. *Atmospheric Chemistry and Physics*, *21*(18), 13973–13996. https://doi.org/10.5194/acp-21-13973-2021

Wang, X., Jacob, D. J., Eastham, S. D., Sulprizio, M. P., Zhu, L., Chen, Q., Alexander, B., Sherwen, T., Evans, M. J., Lee, B. H., Haskins, J. D., Lopez-Hilfiker, F. D., Thornton, J. A., Huey, G. L., & Liao, H. (2019). The role of chlorine in global tropospheric chemistry. *Atmospheric Chemistry and Physics*, *19*(6), 3981–4003. https://doi.org/10.5194/acp-19-3981-2019

Wang, X., Jacob, D. J., Fu, X., Wang, T., Breton, M. L., Hallquist, M., Liu, Z., McDuffie, E. E., & Liao, H. (2020). Effects of anthropogenic chlorine on $PM_{2.5}$ and ozone air quality in China. *Environmental Science & Technology*, *54*(16), 9908–9916. https://doi.org/10.1021/acs.est.0c02296

Wang, Y., Jacob, D. J., & Logan, J. A. (1998). Global simulation of tropospheric O_3 -NO_x-hydrocarbon chemistry: 1. Model formulation. *Journal of Geophysical Research: Atmospheres*, *103*(D9), 10713–10725. https://doi.org/10.1029/98JD00158

Wang, Y., Ming, T., Li, W., Yuan, Q., de Richter, R., Davies, P., & Caillol, S. (2022). Atmospheric removal of methane by enhancing the natural hydroxyl radical sink. *Greenhouse Gases: Science and Technology*, *12*(6), 784–795. https://doi.org/10.1002/ghg.2191

Warwick, N. J., Archibald, A. T., Griffiths, P. T., Keeble, J., O'Connor, F. M., Pyle, J. A., & Shine, K. P. (2023). Atmospheric composition and climate impacts of a future hydrogen economy. *Atmospheric Chemistry and Physics*, *23*(20), 13451–13467. https://doi.org/10.5194/acp-23-13451-2023

Weng, H., Lin, J., Martin, R., Millet, D. B., Jaeglé, L., Ridley, D., Keller, C., Li, C., Du, M., & Meng, J. (2020). Global high-resolution emissions of soil NO_x, sea salt aerosols, and biogenic volatile organic compounds. *Scientific Data*, *7*(1), Article 148. https://doi.org/10.1038/s41597-020-0488-5

Wittmer, J., Bleicher, S., Ofner, J., & Zetzsch, C. (2015b). Iron(III)-induced activation of chloride from artificial sea-salt aerosol. *Environmental Chemistry*, *12*(4), 461–475. https://doi.org/10.1071/EN14279

Wittmer, J., Bleicher, S., & Zetzsch, C. (2015a). Iron(III)-induced activation of chloride and bromide from modeled salt pans. *The Journal of Physical Chemistry A*, *119*(19), 4373–4385. https://doi.org/10.1021/jp508006s

World Chlorine Council https://worldchlorine.org/wp-content/themes/brickthemewp/pdfs/sustainablefuture.pdf

Zhang, J., Wuebbles, D. J., Kinnison, D. E., & Saiz-Lopez, A. (2020). Revising the ozone depletion potentials metric for short-lived chemicals such as CF_3I and CH_3I. *Journal of Geophysical Research: Atmospheres*, *125*(9), Article e2020JD032414. https://doi.org/10.1029/2020JD032414

Zhang, L., Gong, S., Padro, J., & Barrie, L. (2001). A size-segregated particle dry deposition scheme for an atmospheric aerosol module. *Atmospheric Environment*, *35*(3), 549–560. https://doi.org/10.1016/S1352-2310(00)00326-5

Zhu, L., Jacob, D. J., Eastham, S. D., Sulprizio, M. P., Wang, X., Sherwen, T., Evans, M. J., Chen, Q., Alexander, B., Koenig, T. K., Volkamer, R., Huey, L. G., Le Breton, M., Bannan, T. J., & Percival, C. J. (2019). Effect of sea salt aerosol on tropospheric bromine chemistry. *Atmospheric Chemistry and Physics*, *19*(9), 6497–6507. https://doi.org/10.5194/acp-19-6497-2019

Zhu, X., Prospero, J. M., Savoie, D. L., Millero, F. J., Zika, R. G., & Saltzman, E. S. (1993). Photoreduction of iron(III) in marine mineral aerosol solutions. *Journal of Geophysical Research: Atmospheres*, *98*(D5), 9039–9046. https://doi.org/10.1029/93JD00202

Zhu, Y.; Li, W.; Wang, Y.; Zhang, J.; Liu, L.; Xu, L.; Xu, J.; Shi, J.; Shao, L.; Fu, P.; Zhang, D.; Shi, Z. Sources and Processes of Iron Aerosols in a Megacity in Eastern China. *Atmos. Chem. Phys.* 2022, *22* (4), 2191−2202.